Plastic photovoltaic roof tiles

by

Richard Philip Donkin

Thesis presented in partial fulfilment of the requirements for the degree of Master of Engineering in Renewable and Sustainable Energy at the Stellenbosch University

Department of Mechanical and Mechatronic Engineering
Stellenbosch University
Private Bag X1, 7602 Matieland, South Africa

Supervisors:

Dr B. Sebitosi Prof. W. van Niekerk

December 2009

Declaration

By submitting this thesis electronically, I declare that the entirety of the work contained therein is my own, original work, that I am the owner of the copyright thereof (unless to the extent explicitly otherwise stated) and that I have not previously in its entirety or in part submitted it for obtaining any qualification.

Date: 1 December 2009

Abstract

Plastic photovoltaic roof tiles

R.P. Donkin

Thesis: MEng (RSE)

December 2009

This project investigated the feasibility of incorporating photovoltaic cells into plastic roof tiles using injection moulding. Such tiles have the potential to provide robust and distributed electricity contained within the building envelope.

Current-voltage curves of amorphous silicon modules were measured under illumination using the PVPM 2540C power measuring instrument, both before and after moulding. The efficiency after moulding was reduced by 53 % to 88 %, with modules that were heated for longer being degraded more. Thus the duration of exposure to high temperatures affected the extent of performance reduction during moulding. This suggested that faster moulding at a lower temperature or faster cooling could solve the problem.

Economic feasibility was examined by calculating the levellised cost of electricity provided by the tiles. A large-scale development in the Western Cape was simulated using a typical meteorological year of weather data and using the anisotropic diffuse irradiance model of Perez *et al.* (1988). Avoided costs due to replaced roofing, avoided costs due to electricity distribution infrastructure, and Clean Development Mechanism credits were accounted for. The cost of energy calculated was R 11/kWh in 2010 rands, which did not compete with the price of conventional grid-based electricity at R 1.8/kWh. The importance of the cost of balance-of-system components, such as the inverter, and not only of the photovoltaic modules, was highlighted for future cost reductions.

Several clear guidelines for manufacturing photovoltaic roof tiles were discovered. The most important of these was that many bypass diodes make the system more robust.

Opsomming

Plastiek fotovoltaïse dakteëls

R.P. Donkin

Tesis: MEng (RSE)

Desember 2009

Hierdie projek het die haalbaarheid van die integrasie van fotovoltaïse selle in plastiek dakteëls deur spuitvorming ondersoek. Sulke dakteëls het die vermoë om robuuste en verspreide elektrisiteit te lewer, sonder om die gebou se vorm te verander.

Stroom-spanning kurwes van struktuurlose silikon eenhede is onder verligting gemeet met die PVPM 2540C kragmeet instrument, voor en na spuitvorming. Die doeltreffendheid na spuitvorming is met 53 % tot 88 % verminder, met groter vermindering in die eenhede wat langer warm was. Dus het die duur van blootstelling aan hoë temperature die mate van vermindering van doeltreffendheid beïnvloed. Dit het suggereer dat óf vinniger spuitvorming by laer temperature óf vinniger verkoeling die probleem kan oplos.

Ekonomiese haalbaarheid is ondersoek deur die koste van die elektrisiteit wat deur die dakteëls gelewer is te bereken. 'n Groot behuisingsontwikkeling in die Wes-Kaap is gesimuleer deur 'n tipiese weerkundige jaar van weerdata en die anisotroop model vir verspreide ligstraling van Perez *et al.* (1988) te gebruik. Vermyde kostes van vervangde dakteëls, vermyde kostes van elektrisiteit distribusie infrastruktuur en krediete van die Meganisme vir Skoonontwikkeling is in ag geneem. Die elektrisiteitskoste was R 11/kWh in 2010 se randwaarde, wat nie mededingend met die R 1.8/kWh koste van gewone netwerk elektrisiteit was nie. Die belang van die kostes van die res van die installasieonderdele, soos die wisselrigter, en nie net die fotovoltaïse eenhede nie, is beklemtoon vir kostevermindering in die toekoms.

Verskeie duidelike riglyne vir die vervaardiging van fotovoltaïse dakteëls is voorgestel. Die belangrikste van hierdie was dat meer omloopdiodes die installasie meer robuust maak.

Acknowledgements

Much gratitude goes to the Centre for Renewable and Sustainable Energy Studies at Stellenbosch for funding this research.

In addition, this project would not have been possible without the help of several generous people and companies. Thanks go to Lomold for providing use of its highly specialised and unique injection moulding machine, as well as for the helpfulness of everyone encountered there. Tenesol kindly provided samples of unencapsulated crystalline silicon photovoltaic cells. The use of the measuring equipment at the University of Cape Town's electrical engineering department is also greatly appreciated, as well as their time and patience.

Thanks also go to Liesel Steyn for her comprehensive editing of this document.

Contents

List of Tables

List of Figures

Nomenclature

The following symbols and notation are use throughout the document.

Ordinary symbols

C	Interconnection adjustment factor
c	Cost
E	Irradiance / light intensity
I	Current
K_t	Clearness index
k	Boltzmann's constant = $1.380\,650\,3{\times}10^{-23}$ J/K
N	Number of photovoltaic modules
m	Number (general)
n	Non-ideality factor of a diode
P	Power
q	Electronic charge = $1.602\,176\,46{\times}10^{-19}$ C
R	Resistance
s	Angle of tilt
T	Temperature
V	Voltage
V_T	Thermal voltage at the temperature T
x	Distance
Z	Zenith angle of the sun

α	Optical absorption coefficient
β	Temperature coefficient of efficiency
η	Efficiency
ρ	Albedo
θ	Angle of incidence of light

Subscripts

a	Ambient
DNI	At direct normal incidence
L	Additional (current) under illumination
m	At the maximum power point
NOCT	At nominal operating cell temperature, under nominal terrestrial environment conditions
nom	Nominal
o	At diode saturation with a small reverse bias
OC	Open-circuit
P	Parallel
pk	Peak
S	Series
SC	Short-circuit
surface	At the surface
STC	At standard test conditions

Notation

$\overline{x}$	The overbar represents the mean.
σ_x	The subscript to a sigma represents the standard deviation.
$\mathbb{E}[x]$	The blackboard bold $\mathbb{E}$ represents the expected value.
Δx	The delta represents a change due to one or more factors.

List of abbreviations

The following abbreviations are used throughout the document.

a-Si	amorphous silicon
AM	air mass
BIPV	building integrated photovoltaics
c-Si	crystalline silicon
CDM	Clean Development Mechanism
CIGS	$CuGa_{1-x}In_xSe_2$
CVD	chemical vapour deposition
DNI	direct normal incidence
EU	European Union
EVA	ethylene-co-vinylacetate
FF	fill factor
I-V	current-voltage
III-V	semiconductor made from groups III and V of the periodic table
ITO	indium tin oxide
MPP	maximum power point
NOCT	nominal operating cell temperature
NPV	net present value
OEM	original equipment manufacturer
PECVD	plasma-enhanced chemical vapour deposition

PEN	poly-ethylene-naphtalate
PET	poly-ethylene-terephtalate
PV	photovoltaic
PVC	poly-vinyl-chloride
SABS	South African Bureau of Standards
SANS	South African National Standard
STC	standard test conditions
TCO	transparent conducting oxide
TMY	typical meteorological year
μ**c-Si**	microcrystalline silicon
USD	United States dollars
UV	ultraviolet light

1 Introduction

1.1 Project concept

This project investigated the feasibility of plastic photovoltaic roof tiles, with reference to a South African context. The future goal is to replace conventional concrete roofing tiles with tiles made from recycled plastic. Moreover, the tiles are to incorporate photovoltaic (PV) cells and be connected together. This will allow a roof that is structurally unmodified to produce electricity for the occupants of the building.

There are a number of unsolved issues, however, which currently prevent the idea from being implemented commercially. Initially, the PV cells need to be incorporated into the roof tile securely and cost effectively. The incorporation method tested in this project was the necessary step of injection moulding. The Lomold (2009) moulding process was used, but it produced high temperatures and pressures which could be damaging to the cells. After incorporation, both the cells and the tiles need to withstand severe weathering and the cells should continue to work electrically. The design of the tile needs to allow light through to the PV cells while still protecting them from mechanical, optical and chemical damage.

Nevertheless, there are numerous benefits to be expected from the tile's production and widespread use. This is particularly true for South Africa, as explained below.

1.2 Motivation for the concept

Currently, photovoltaic roof tiles are in production and limited use in other countries, such as Switzerland, Germany, the United States of America and Japan (Posnansky *et al.*, 1998). These tiles are used in conjunction with an inverter to produce power for the local electrical appliances. At some times of the day the power produced is greater than the power used by the household, and then the excess power is fed back into the regional electricity grid, resulting

in a deduction from the bill of the household or business. This is done in a safe way by using inverters that "automatically disconnect the PV system from the line if utility power fails" (U.S. Department of Energy, 1999).

Photovoltaic power has the potential to benefit South African electricity provision greatly. According to the Earth Policy Institute (1999), Germany installed a photovoltaic capacity of more than 1 GW in 2007 alone — including other installations as well as roof tiles. This is a significant amount of solar power, especially if it is applied to the state of the South African power grid. Eskom, the electricity provider in South Africa, is operating at less than a 10 % power capacity margin at peak times of the day, and is below its planned margin (Eskom, 2009*b*). As a result Eskom is making regular use of planned power outages, referred to as load shedding, which are disruptive to industry and commerce. Eskom's grid capacity of about 40 GW would benefit greatly from a PV-peak reduction in load of 1 GW, which could be provided by a PV market similar to that of Germany. Thus distributed solar power has the potential to alleviate Eskom's problem of the peak electricity demand on the regional grid.

Another benefit of solar power in general is its renewable nature. The 92 % dominant source of electricity in South Africa is coal-fired power stations (SouthAfrica.info, 2009). Coal-fired power generates approximately 0.95 kg of carbon dioxide per kWh of electricity (U.S. Department of Energy, 2000). This means a gigawatt of solar power, over a year's worth of 4 strong daylight hours per day, could save 1.4 Mt of carbon dioxide from entering the atmosphere. This is in line with the Millennium Development Goals of the United Nations: Goal 7, Target 1 is to "Integrate the principles of sustainable development into country policies and programmes and reverse the loss of environmental resources." One of the main components of this target is to contain rising greenhouse gas emissions (United Nations, 2000).

There are problems, though, with the currently available photovoltaic tiles. Firstly, the tiles are expensive, and the Earth Policy Institute (1999) estimates that the cost of photovoltaic electricity in 2006 was 3.84 United States dollars (USD) per kWh, averaging the initial costs over the lifetime of a panel. This is in sharp contrast to Eskom's tariffs in 2009 of less than 1 rand, or less than 0.1 USD, per kWh (Eskom, 2009*c*). Secondly, the tiles are usually not integrated well into the roof. Either they consist of separately manufactured PV modules added to roof tiles; or they are have a different size from the tiles and do not fit nicely into the normal tiling pattern (see for example Bahaj, 2003). Usually additional reinforcements are required to hold PV tiles. Thirdly, the electrical connection of current photovoltaic tiles is difficult and cumbersome (Rautenbach, 2008; Posnansky *et al.*, 1998).

Plastic photovoltaic tiles have the potential to address these problems. Plastic is relatively inexpensive and can be moulded into shape easily. Moreover it is possible to produce plastic surfaces that are consistent and smooth, and

which thus may be suitable as the substrates for photovoltaic cells. This would significantly reduce the costs of the tiles. In addition, plastic is flexible and lends itself to clip-together assembly of modules. This could potentially simplify the access for maintenance and fault-finding.

It can be seen that recycled-plastic photovoltaic tiles could have benefits to Eskom, the economy and the environment. These benefits suggest subsidies to those consumers and businesses wishing to try the tiles once they are in production. This would hasten the adoption, and the costs of the subsidies should soon be recovered from the power saved due to the photovoltaic installations. A form of subsidy that has found success in other countries is the feed-in tariff, and this could also be considered in South Africa for PV roof tile installations.

1.3 Proposed end product

Considering the South African market and the purpose of making a substantial electricity contribution, the following characteristics are wanted for a marketable PV roof tile system.

- The tiles should be able to be installed easily in the same way as standard tiles, although the electrical connections may need to be done by an electrician.
- A collection of tiles to be installed on a domestic roof should be able to provide enough electricity so that it is useful for household appliances.
- The tiles are expected to be integrated into a battery and alternator system.
- The system should be robust so that, if a few tiles fail, it will still work at a proportionate level of effectiveness.
- The tiles should meet the relevant building regulations of the South African Bureau of Standards (SABS).
- The tiles should have a lower cost than current domestic PV solutions in South Africa.

Current PV roof installations are complicated to install and alter the normal roof of the building. (This is discussed further in Section 2.7.2.) This is aesthetically unpleasing and makes them expensive. Thus it is important that the roof tile is able to fit into a standard roof tiling setup.

The tile should also be made of recycled materials. This will improve its environmental impact even further than is done by producing solar-generated

electricity. It is proposed to incorporate the PV cells into recycled plastic roof tiles using an injection moulding process developed by Lomold. The effect of this process on the PV cells will be investigated in this project.

1.4 Scope of this project

This main focus of this project was the feasibility of injection moulding as a process to incorporate PV cells into roof tiles. Thus, the scope did not directly include the design of the shape and composition of the roof tile. The shape was considered in an indirect way in terms of the size of the module, and the composition in terms of an estimate of what will be required for the final roof tile.

Specifically, the following questions were answered by this project for at least one type of PV cell.

- How possible is it to incorporate cells into the moulding process?
- To what extent is a cell damaged by the moulding process?
- To what extent are the electrical characteristics of a cell altered by the moulding process?

A literature review helped to choose which PV cells to use. It helped find which technologies would probably be suitable for incorporation into an injection moulding process.

2 Literature review

The literature was reviewed with the main goal of this project in mind: to incorporate PV cells into plastic roof tiles using injection moulding. The big picture presented includes the total design of the tiles and their electrical systems. The design of the tiles includes the photovoltaic technology, the mechanical protection, the encapsulation process, and the electrical connections. The design of the systems includes the prediction of performance and sizing of the array, as well as the other electrical parts needed (such as batteries). Previous work on solar roofing is also discussed.

2.1 Photovoltaics

2.1.1 Physical principle

Photovoltaics is based on photons exciting electrons in a semiconductor. The electrons are then free to create a current. The voltage to move the electrons is provided by a p-n junction.

Bandgap and electron excitation

A semiconductor has a valence band, where electrons rest when they have no energy, and a conduction band, where electrons may be found when they are excited. When electrons are still in the valence band they are tightly bound to their atoms' nuclei, but when they are in the conduction band they are more free to move around as electrical current. 'Holes', vacant electron spaces in the valence band, can also move about in the same way. The 'bandgap' is the amount of energy required to excite an electron from the valence band to the conduction band. Semiconductors have medium-sized bandgaps on the order of 1 eV.

The convenience of the medium size of the bandgap is that some photons carry about the same amount of energy. Thus photons are able to give their energy

to electrons when the photons enter the semiconductor, exciting electrons into the conduction band (Jaeger *&* Blalock, 2003). A photon needs a high enough energy to do this, which corresponds to a high enough frequency. If a photon is at too low a frequency it cannot excite an electron. If a photon is at a very high frequency it may excite an electron but the rest of its energy will be dissipated, which is a waste.

Some semiconductors have a higher 'optical absorption' than others, even though their bandgaps are similar. One important reason for this is the momentum of the electrons in the valence and conduction bands. If the electron needs to gain or lose momentum in addition to energy as it jumps the bandgap, it then becomes difficult for a photon to excite it. (Photons do not have momentum.) A 'direct bandgap' does not require a change of momentum, whereas an 'indirect bandgap' does.

Current generation

Once the electrons have been excited they usually diffuse through the semiconductor until they are recombined; that is until they drop back to the valence band. If however, the electrons reach an electric field then they are swept along by it and form a 'drift current'.

To allow the electrons enough time to reach the electric field it is necessary for them to have a long 'diffusion length' or 'diffusion lifetime' for the minority charge carriers (Miles *et al.*, 2005). The minority carriers are electrons in a p-type semiconductor or holes in an n-type semiconductor. The carrier lifetimes can be kept high by only doping the semiconductors lightly, but there is a trade-off because more heavily doped semiconductors have lower resistance in their bulk and in their contact with metals.

It is well known that a small electric field exists over a p-n junction, and this provides the field in PV cells. The field sweeps up the excited electrons that drift into it and adds them to its drift current, which would otherwise be very small. The drift current flows from the n-type to the p-type semiconductors[1], in the opposite direction to a voltage applied over the junction. This means power is generated as long as the applied voltage is not so much that the junction's 'diffusion current' overwhelms the drift current.

Finally the electrons pass through an external circuit. When electrons arrive back at the p-type semiconductor they recombine with holes, having lost their energy in the circuit.

[1]The current flow direction is defined as opposite to the electron flow direction. Thus, drift current electrons flow from the p-type to the n-type semiconductors.

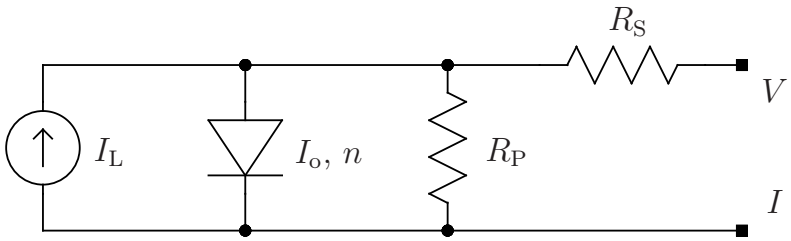

Figure 2.1: Schematic diagram of the model for a PV cell

Note: The resistances are sometimes ignored and omitted.

2.1.2 Equivalent model

The current through a PV cell can be modelled in more or less complicated ways, depending on the needs. For power generating applications the following five-parameter model is sufficient (de Blas *et al.*, 2002).

$$I = I_{\mathrm{L}} - I_{\mathrm{o}} \left[\exp\left(\frac{V + IR_{\mathrm{S}}}{nV_T} \right) - 1 \right] - \frac{V + IR_{\mathrm{S}}}{R_{\mathrm{P}}} \tag{2.1}$$

Here I is the operating current and V is the operating voltage. The parameters of the model are:

I_{L} , the photocurrent;
I_{o} , the saturation current;
R_{S}, the series resistance;
R_{P}, the parallel resistance; and
n , the diode non-ideality factor.

The thermal voltage is $V_T = kT/q$, where k is Boltzmann's constant, T is temperature and q is the charge of a single electron. The model is shown schematically in Figure 2.1.

The only part of the model that differs from a normal diode is the presence of I_{L}, which is generated in proportion to the irradiance. Irradiance is how much light strikes the cell. R_{S} is due to the metal contacts and the conduction in the bulk of the semiconductor, and R_{P} is due to internal defects in the semiconductor. The non-ideality factor $n \approx 1$ for a normal diode, but it is usually higher in PV cells.

A second diode may be placed in parallel with the first one to model currents at low voltages and low levels of irradiance. Its effects are insignificant, however, at the voltages and irradiance levels used for generating power.

This model is not fixed. The values of the parameters change according to various conditions, especially irradiance and temperature.

2.1.3 Irradiance effects

As the amount of light striking the cell increases, the number of excited electrons increases in direct proportion, and so the current. This means I_{L} increases proportional to irradiance, measurable as an increase in the short-circuit current I_{SC}.

The open-circuit voltage V_{OC} is determined by the point where the exponential term in Equation (2.1) cancels I_{L}. Thus, V_{OC} increases logarithmically with irradiance as I_{L} increases linearly.

The combination of linear increase of I and logarithmic increase of V results in a more-than-linear increase of power with irradiance. In other words, a cell's efficiency increases as it is exposed to brighter light. This is exploited by solar concentrators which can operate at very high efficiencies.

Temperature effects

The performance of PV cells degrades as temperature rises. As the temperature of the semiconductor increases, the electrons become more thermally excited. As a result the saturation current I_{o} increases exponentially with temperature, draining more of the photocurrent I_{L}. At the same time V_{OC} decreases linearly. The combined effects of decreasing I_{SC} and V_{OC} cause the degradation of performance, though V_{OC}'s effect dominates to make the decrease almost linear (Radziemska, 2003).

The decrease in efficiency is commonly represented by a simple linear expression (Skoplaki *&* Palyvos, 2009):

$$\eta = \eta_{\mathrm{STC}} \left[1 - \beta(T - T_{\mathrm{STC}})\right] \tag{2.2}$$

where η is the efficiency and β is the temperature coefficient of efficiency. Standard test conditions (STC) are 1000 W irradiation at 25 °C and AM1.5. The air mass (AM) refers to the spectrum that solar radiation obtains after travelling through a distance of air 1.5 times the average thickness of Earth's atmosphere (Swanepoel, 2007:115).

The value of β differs widely between different PV technologies and to a lesser extent between manufactured items of the same technology. Well-known examples are $\beta = 0.0045\,\mathrm{K}^{-1}$ for crystalline silicon and $\beta = 0.0026\,\mathrm{K}^{-1}$ for amorphous silicon.

Silicon-based PV cells have significant temperature coefficients. They are usually unsuitable for solar concentrators because the increases in efficiency due to irradiance are outweighed by the decreases due to the higher temperatures.

2.2 Technologies

The range of PV technologies already in the market and still under development is impressive, and difficult to organise in a straightforward way. Here, the technologies will be classified first according to raw materials and then, within those groups, according to manufacturing processes. A good review of the technologies is given by Miles *et al.* (2005), with more detail than is extracted below for most technologies.

2.2.1 Crystalline silicon

Photovoltaic cells made out of crystalline silicon were the first cells to be sold in a large scale on the market, and they still dominate the market today (Maycock & Bradford, 2006). Their strength is durability under harsh optical and temperature conditions. Their weaknesses are brittleness and being expensive to produce.

Crystalline silicon (c-Si) cells need to be quite thick and very pure. The wafers need to be on the order of 350 μm because c-Si has a low optical absorption. This requires a large amount of silicon considering that large areas need to be manufactured to generate significant power. [The low absorption is because c-Si has an indirect bandgap (Miles *et al.*, 2005).] Moreover, the silicon is very pure and requires a fairly high energy input to produce. These factors add to the cost of the cells.

There are a few ways to make crystalline cells but they share some common points. All are manufactured as wafers which act as substrates, after which they are doped by bombardment with ions. All the structures have large crystal grains and are exceedingly brittle; so they need to be encapsulated in glass to provide structural strength.

Monocrystalline silicon

The single-crystal cells are identifiable by their unvaried colour and their round shape. The cells are produced by sawing a large ingot into slices. The cylindrical ingot is usually manufactured using the Czochralski process which is slow, precisely controlled and energy intensive.

Multicrystalline silicon

The multi-crystal cells are identified by their mottled shades of colour and their square or other geometrical shapes. They are also made from sawing

an ingot, but the ingot is cast all at once instead of being slowly grown by the Czochralski process. The result is a slightly less energy intensive process which is also significantly quicker. The disadvantage of multiple crystal grains in a cell is that recombination of electrons and holes tends to happen at grain boundaries. This means that multicrystalline cells are less efficient.

Ribbon-manufactured silicon

A different kind of multicrystalline cell can be produced by drawing a film from a bath of molten silicon. The result is essentially the same as sawing from a multicrystalline ingot, except that the resulting efficiency is not quite as good. The major advantage is that there is no waste of silicon due to dust ('kerf') produced during sawing.

There is a variety of ways to draw out the silicon sheets, which will not be covered here. For more detail refer to Miles *et al.* (2005).

2.3 Thin films

Some forms of semiconductor have higher optical absorption (for example because they have a direct bandgap). They can make cells that are much thinner than crystalline silicon and still absorb most of the incoming light. These may be referred to as thin-film PV cells.

Thin-film semiconductors also generally have bandgaps close to the optimum bandgap (Miles *et al.*, 2005). The optimum bandgap for the solar spectrum is about 1.5 eV. A large proportion of solar light is above the frequency that corresponds to this, so it can excite electrons by 1.5 eV. However, the light is not too far above what is needed for the bandgap, so not too much is wasted. Crystalline silicon has a bandgap of about 1.1 eV, but many thin films do better than this.

Thin films are manufactured in ways that may allow them to be flexible, or at least not as brittle as crystalline silicon. They are made of all sorts of semiconductor raw materials, most of which are discussed here. Silicon-based thin films (amorphous and microcrystalline) were the main focus of this project, though, and are discussed in Section 2.4.

2.3.1 III-V based thin films

Semiconductors can be made from a crystal structure with a combination of elements from group III and group V of the periodic table (Miles *et al.*, 2005).

Examples are GaAs and InP. These semiconductors were first used for PV cells in space. They were expensive but durable and efficient for their weight. They are still very expensive and are not widely used in terrestrial power generation.

III-V semiconductors produce the most efficient cells available, operating at efficiencies greater than 35 %. They are able to withstand high temperatures without degradation, as well as high levels of cosmic radiation. They have true direct bandgaps.

The cells are produced using 'liquid phase epitaxy' or 'metalorganic chemical vapour deposition'. These methods work by depositing layers of semiconductor in sequence, which are doped individually.

One of the key advantages of layer-by-layer manufacture is that multiple-junction cells can be made. For example, a double-junction ('tandem') cell consists of two different PV cells, one laid on top of the other so that they are connected electrically in series. The upper layer has a higher bandgap, so it converts high-frequency light with little waste but lets lower-frequency light through completely. The lower layer has a lower bandgap, so it is able to convert the remaining low-frequency light, and does so with little waste.

Double-junction and triple-junction cells are common because they are capable of higher efficiencies. However, the extra complexity makes it hard to design the cells and requires tighter manufacturing tolerances. The currents produced need to match because the layers are in series, otherwise one layer will limit the effectiveness of the other layer.

The materials used in III-V cells are expensive (compared to silicon), so the cells are often used in concentrators. This allows a small cell to produce electricity using the light from a larger area. The cells are appropriate for this because they operate effectively at higher temperatures and, as explained above, their efficiencies are higher at larger irradiance levels.

Some commonly used semiconductors are GaAs, GaP, GaSb and $GaInP_2$. Other semiconductors based on InP are unusually resistant to radiation and good for space applications: InGaAs, InGaP, AlGaAs and AlInGaP. The expensive materials are often grown on a Ge substrate.

2.3.2 Cadmium telluride thin films

Thin films with direct bandgaps can be made using a combination of CdTe and CdS. These are deposited by sublimation and vapour movement across a very short distance.

The films have been criticised because the long-term effects of Cd on humans and other life are unknown. However, the following should be kept in mind.

First, CdTe is a stable compound and insoluble. Second, Cd is a byproduct of zinc manufacturing and is usually disposed of by safe dumping anyway.

CdTe films are commercially available and were the second most popular thin films in 2005, second to amorphous silicon (a-Si).

2.3.3 Chalcopyrite thin films

The chalcopyrites, also with direct bandgaps, are made from groups I, III and VI of the periodic table. Examples are $CuInSe_2$, $CuInS_2$ and $CuGa_{1-x}In_xSe_2$. The latter is often referred to as CIGS. It has received much publicity and has shown great potential. However, its mass production processes have not been worked out fully and there are many different production methods.

One of the benefits of CIGS is that it is very stable and does not degrade over time (Grama, 2007:17).

2.3.4 Dye-sensitised cells

A very different type of PV cell can be made using 'photo-electrochemical' principles, different from the solid-state principles other cells use. The basic structure is a liquid electrolyte between two electrode sheets. One electrode is made of TiO_2 coated with a dye; the dye being a transition metal complex. The other electrode is a layer of pyrolithic platinum.

These cells are not in commercial production and show low efficiency.

2.3.5 Organic cells

Semiconductors called 'organic' are carbon-based. They are made out of polymers or derivatives of fullerene (C_{60}). The cells are layered in similar ways to the other semiconductor cells.

Organic PV cells are not yet in commercial production. They show low efficiency and are not stable over long periods of time.

2.4 Silicon-based thin films

Silicon can be deposited onto a substrate to form different structures on a continuum between amorphous and microcrystalline. These will be discussed here as well as their deposition processes.

Silicon-based thin films were chosen for this project as the type of PV cell to be tested with injection moulding. Consequently they needed to be understood more thoroughly, so more space is dedicated to them here.

2.4.1 Amorphous silicon

'Amorphous' means not having a crystalline structure. This refers to a disordered arrangement of atoms that are not organised into a lattice. Silicon can form this kind of structure under certain conditions but, because there is no lattice, some of the Si atoms' bonds will be left dangling. To make the amorphous structure stable it is necessary to passivate these dangling bonds with hydrogen ions. That is why amorphous silicon is deposited using plasma-enhanced chemical vapour deposition (PECVD).

Amorphous silicon (a-Si) has an almost-direct bandgap (which is notable because c-Si does not). Its bandgap is about 1.7 eV (Miles *et al.*, 2005). The result of this is a high optical absorption coefficient: $\alpha > 10^5\,\mathrm{cm}^{-1}$. By contrast, c-Si has an optical absorption $\alpha \approx 100\,\mathrm{cm}^{-1}$, or about 1000 times less.[2] An a-Si film could theoretically be 1000 times thinner than a c-Si wafer and save a corresponding amount of silicon.

Unfortunately, a-Si also has a small charge carrier diffusion length. This makes it hard for electrons to diffuse far and reach the electric field of the p-n junction. The solution to this is to let the light be absorbed *within* the electric field. An intrinsic silicon ('i') layer is deposited between the p-type and n-type layers and is significantly thicker than them. Most of the light is absorbed in this i layer and the electrons are immediately swept up by the electric field. Still, the entire a-Si cell needs to be kept thinner than about 4 μm to generate current in a satisfactory way (Shah *et al.*, 2004).

A disadvantage of a-Si is its deterioration when exposed to light, called 'photodegradation' or the 'Staebler-Wronksi effect'. The degradation is logarithmic; that is it does not ever stop but becomes insignificant (Shah *et al.*, 2004). The degradation can be reversed by thermal annealing at temperatures above 65 °C when in use (Gottschalg *et al.*, 2004). Annealing can also be done in the laboratory at a faster rate at 150 °C (Filonovich *et al.*, 2008). The annealing when in use means that a-Si performs better in summer than in winter as long it is heated up above 65 °C by the sun in summer. This is applicable to South African conditions.

[2] Light intensity decays exponentially as it passes through a material as follows:

$$E = E_{\mathrm{surface}} \exp(-\alpha x)$$

where x is the distance into the material at which the light intensity E is observed (Swanepoel, 2007:133). Thus the penetration depth can be thought of as $1/\alpha$. A higher α means higher absorption.

Multi-junction PV cells can be made by alloying the a-Si to change its bandgap for different layers. It can be alloyed with Ge for a smaller bandgap (for lower layers in the stack), or alloyed with C for a larger bandgap (for higher layers in the stack).

2.4.2 Microcrystalline silicon

Using the same process as for a-Si but under different conditions, silicon can form a multitude of micrometre-sized crystals instead of an amorphous structure. This is called microcrystalline silicon (μc-Si). Variations of the structure are called nanocrystalline and polymorphous (as by Filonovich *et al.*, 2008), and protocrystalline (as by Ishikawa & Schubert, 2006).

The best material properties for photovoltaics are achieved near the transition between an amorphous and a microcrystalline structure. The structure is then small crystals embedded in an amorphous base (Ishikawa & Schubert, 2006). This structure has a high photosensitivity as well as a high diffusion length. A fully microcrystalline structure, by contrast, has an even higher diffusion length but a lower photosensitivity (becoming more like multicrystalline silicon).

Microcrystalline silicon does not suffer from photodegradation if it is made in the right way (Shah *et al.*, 2004). Its bandgap is about 1.1 eV, or the same as c-Si and less than a-Si. This makes it good as the lower layer in a tandem cell. The upper a-Si layer should then be given excess current capacity, so that when it degrades it matches the current of the μc-Si layer (Gordijn *et al.*, 2006). Double-junction cells made using these two different layers are sometimes called 'micromorph' cells.

2.4.3 Deposition

The feedstock for thin-film silicon is SiH_4 (silane) gas, not purified elemental silicon. It is deposited using chemical vapour deposition (CVD) with SiH_4 mixed with H_2. A high temperature needs to be sustained so that the amorphous structure forms correctly. It also helps to used 'plasma-enhanced' CVD so that extra energy is added via the flux of ions (Verkerk *et al.*, 2009).

The dangling Si bonds are passivated by H ions. The aim is to form SiH items and not SiH_2 during the process (Tanda *et al.*, 2005). The reason is that SiH_2 is not as stable and contributes to photodegradation.

The feedstock dilution is a control parameter and its mol concentration may be varied between about 2 % and 50 % (Filonovich *et al.*, 2008). A lower dilution smaller than about 5 % produces μc-Si, and a higher dilution produces a-Si. In the transition polymorphous, nanocrystalline or protocrystalline silicon can be formed.

Slow deposition rate

Perhaps the greatest unsolved problem with the production of silicon thin films is the slow deposition rate. The films are grown as slowly as 0.1 nm/s (Shah *et al.*, 2004). This means 50 minutes for an a-Si layer of 0.3 μm and much longer for a μc-Si layer of 1 μm to 2 μm. Deposition could be made faster by increasing the plasma excitation power, but this is not done because it causes more SiH_2 items instead of SiH items.

There are various other ways researched to speed up the film growth rate. These include increasing the plasma excitation frequency into the radiofrequency range or even the 'very high frequency' range, using microwave plasmas, and using higher pressures (Shah *et al.*, 2004). 'Hot wire' CVD has also been used (Filonovich *et al.*, 2008).

High substrate temperature

Deposition is typically done at temperatures of about 200 °C, for example by Rath *et al.* (2008) on aluminium and Tanda *et al.* (2005) on polyimide. Using cheaper plastics than polyimide would allow more widespread use of a-Si, but 200 °C is too hot for them and would melt them. If the deposition temperature is decreased then the a-Si has more structural disorder, which degrades all its photonic and electrical characteristics (Koch *et al.*, 2001).

The reason for the structural disorder is explained by Verkerk *et al.* (2009). When deposited on a substrate at a lower temperature, the SiH_3 molecules with dangling bonds have less energy and less surface mobility. Plasma carries extra energy to the surface through its ion flux, but there is less flux and less ion energy at lower temperatures. The lower temperature near the surface results in a higher gas density, so that more ion collisions occur and the ions have less energy as a result.

The a-Si structure may be improved in low-temperature deposition by decreasing the concentration of SiH_4 in H_2. The relatively higher amount of H_2 creates a higher ion flux as well as a higher ion energy, since H ions require more energy to create.

Deposition order

There are two configurations for thin-film cells, called 'substrate' and 'superstrate'. A substrate configuration deposits the semiconductor on an opaque sheet, and transparent layers are laid on top. An example is UniSolar's stainless steel sheet meant for roof mounting (Shah *et al.*, 2004). A superstrate configuration deposits the semiconductor on a transparent sheet. Actually,

Substrate	Transparent superstrate
Reflective layer	
	TCO[3]
Semiconductor layers	Semiconductor layers
TCO	TCO
	Reflective layer
Transparent mechanical protection	Mechanical protection
(a) Substrate	(b) Superstrate

Figure 2.2: Order that layers are laid in different thin film configurations

[3]This TCO needs to remain stable during PECVD. The common indium tin oxide (ITO) is not appropriate, though ZnO is suitable (Shah *et al.*, 2004).

the sheet (which is still technically called a substrate) is coated with a transparent conducting oxide (TCO) first. Finally a mechanically protective opaque layer is added over the semiconductor. An example is Fuji Electric's polyimide sheet described by Tanda *et al.* (2005). The orders in which layers are added in the superstrate and substrate configurations are shown in Figure 2.2.

2.5 Production issues for silicon-based thin films

Producing silicon film PV cells requires an understanding of more than just the semiconductor physics. The films do not exist in isolation and care has to be taken with how they interact with their environment. The right substrates have to be chosen, the encapsulation needs to be durable, and their electrical interconnections need to be strong. Finally, the production needs to be as cheap as possible.

Throughout the rest of this document, reference to a-Si cells includes the implicit case of a-Si/μc-Si double-junction cells.

2.5.1 Substrates

Amorphous and microcrystalline silicon are usually deposited on glass in a superstrate configuration. However, they can also be deposited on stainless steel or aluminium in a substrate configuration, and are even sometimes deposited on plastic.

The advantages of a glass substrate are that it is mechanically robust and long-lasting. These characteristics make glass very popular, despite its disadvantages. Glass is heavy, which makes it expensive to transport and expensive

to support physically when installed. Glass is also not flexible, which makes it difficult to use for PV applications on curved surfaces. This has been done, though, by Matsuoka *et al.* (1990) using a complicated laser scribing mechanism.

The advantages of a plastic substrate are that it is cheap, light and flexible. Plastic also has significant weaknesses, however. Most plastics are well known to embrittle and discolour with exposure to ultraviolet light (UV). Most plastics are also not able to withstand the high temperatures used in CVD.

The problem of the high deposition temperature can be solved in the following ways. The temperature can be lowered so as to be suitable for plastics by increasing the amount of H_2 during deposition, as explained in Section 2.4.3. This is effective to temperatures as low as about 100 °C, but not below as yet (Koch *et al.*, 2001). Alternatively, the semiconductor can be deposited on a sacrificial substrate and transferred to a plastic sheet. This is described by Rath *et al.* (2008) where the Helianthos project used aluminium foil for the sacrificial substrate.

Some plastics used have been:

- poly-ethylene-naphtalate (PEN) (Filonovich *et al.*, 2008; Haug *et al.*, 2009; Söderström *et al.*, 2009),
- poly-ethylene-terephtalate (PET) (Haug *et al.*, 2009; Söderström *et al.*, 2009; Ishikawa *&* Schubert, 2006), and
- polyimide (Filonovich *et al.*, 2008; Tanda *et al.*, 2005; Yoshida *et al.*, 2000) which is expensive and can withstand high temperatures.

2.5.2 Encapsulation

The purposes of the module encapsulation are (a) to allow light through to the cells, and (b) to protect the cells against mechanical damage. The latter includes sealing against corrosion, especially by water. The encapsulation should not suffer from UV degradation and should protect the cells from it too if necessary.

Often the substrate forms one side of the encapsulation, but the other side needs to be chosen carefully and bonded on properly.

Light acceptance

The way the transparent cover for the PV cells is designed can actually improve their acceptance of light. This can be thought of in terms of minimising

reflection. All the layers above the cells (for example the TCO) have reflecting effects, but by far the dominant effect in glass-covered modules is by the air-glass interface (Balenzategui *&* Chenlo, 2005). This is mainly due to the large difference between the index of refraction of air and that of glass.

One of the main design aims is to diffuse the incoming light so that acceptance is improved at angles other than perpendicular. A roughened *outer* surface helps with this. The texture may be random or periodic in two dimensions, but for good results the feature size or period should be on the same scale as the light wavelength (Söderström *et al.*, 2009).

There are other tools apart from a roughened surface. Light trapping can be optimised precisely by adjusting the thicknesses and indices of refraction of the layers of the module. This is mostly effective in thin films where all the layers are made with high precision. As a different approach, it is interesting to note that narrow strips of a-Si perform better at high incidence angles than broad strips do (Balenzategui *&* Chenlo, 2005).

Mechanical protection

The mechanical and chemical robustness of the encapsulation is more important than photodegradation of the a-Si in many real-world applications. There are all sorts of potential problems, as illustrated by van Dyk *et al.* (2007).

Ethylene-co-vinylacetate (EVA) is often used as the 'pottant' (glue) for PV modules, despite its weaknesses (Czanderna *&* Pern, 1996). The polymer chains in EVA undergo scission and crosslinking under UV exposure. This forms polyenes and acetic acid, with the negative effect that acetic acid is a catalyst for further UV degradation and may corrode metal connections. Stabilisers are added to EVA to prevent UV degradation, but they are sacrificial and become used up after long exposure. Moreover, the stabilisers need to be mixed in the proper proportions to be useful.

Cerium-doped glass acts as a UV screen which protects the EVA and other polymers. It also has the beneficial effect of diffusing light (Balenzategui *&* Chenlo, 2005).

Better pottants than EVA are ideally needed. When it cracks, ingress of water and corrosion can completely destroy a substrate, as in van Dyk *et al.*'s case for aluminium (2007). It may be that thin films on plastic substrates do not need a pottant, but can be sealed by plastic welds around the edges. It appears that PowerFilm's modules (described in Section 3.2.2) used this approach.

2.5.3 Mechanical strain

Building-integrated PV cells may be subjected to stresses as they form part of the building structure. Jones *et al.* (2002) investigated the effects of strain on a-Si cells, which were found to deform plastically but to resist electrical damage fairly well.

No damage to the electrical performance was recorded due to compressive strain. Under tension, there was no recorded damage until a strain of 0.75 %. This is quite large tension, corresponding for the tested cells to a small 8.3 mm radius of curvature. After 0.75 % strain, microscopic damage occurred (not macroscopic cracking). V_{OC}, I_{SC} and FF were reduced. In addition the cells started acting less like diodes and more like resistors, becoming conductive under reverse bias.

This strain resistance of a-Si cells is more than enough to survive thermal expansion of the substrate. For example, stainless steel has a coefficient of linear thermal expansion of $14.4–17.7\times10^{-6}$ m/m·K. For it to achieve 0.75 % expansion would require a temperature increase of 433–521 °C, which is not likely in practice.

The strain resistance may not be enough for surfaces that will be highly curved after production. Also, despite being far more flexible than c-Si, a-Si cells are not appropriate for highly flexible or load-bearing substrates.

2.5.4 Interconnection

It is necessary to lay PV cells in series to increase the output voltage. A higher voltage allows for less current to deliver the same power, which means thinner interconnection wires may be used.

An advantage of thin-film cells is that a number of them can be created on a single substrate and connected 'monolithically'. Most manufacturers do this. It allows modules to have high output voltages without soldered connections and allows even small modules to have high voltages.

2.5.5 Economies of scale

Thin-film silicon, especially a-Si, is not as cheap yet as it has been predicted to be. One of the biggest factors limiting its cost reduction is the small scale of production. Low sales volumes mean higher overheads and higher distribution and marketing costs per module.

One reason for the low-scale production is the long deposition time required for a-Si. It forces many manufacturers to use a batch process instead of a

continuous process. In addition it takes longer to recover once-off initial engineering costs and costs of machinery. This is a likely reason for the large sizes of most modules which make them inappropriate for roof tiles (see Table 3.1 on page 32 for some examples).

Even apart from the once-off costs, the main part of the cost of thin-film PV cells is not in the semiconductors. Zweibel (1999) examined material costs and found that the expensive CdTe material formed only 10 % of the total materials cost for First Solar's cells; with the rest being the encapsulation, the packaging and the module structure. Clearly costs need to be reduced in a number of areas.

2.6 System design issues

Designing a system of PV modules to power an application requires additional knowledge. Some relevant topics will be discussed here with a focus on a-Si modules, although the topics really apply to all PV cells.

A universal problem for consistent design is the apparently random variation of characteristics of components. This is particularly relevant to a-Si modules: Gottschalg *et al.* (2004) show how efficiency can vary by as much as a factor of 2 between cells of the same technology. The variation within a given brand is also noticeable, though smaller.

2.6.1 Energy yield prediction

Predicting how much energy a given array of PV modules will produce is difficult to do accurately. It requires predicting the irradiance on the modules in their environment and then predicting their efficiency in converting it to electrical energy. The irradiance and efficiency can be predicted if weather conditions are known, or a variety of algorithms can be used to estimate average weather conditions.

Irradiance prediction

The irradiance on a module is determined by the position of the sun (which is predictable) as well as the general weather conditions (which are less predictable). If there were no intervening atmosphere, then the total ('global') irradiance could be determined purely by geometry and the knowledge of the sun's position through the day. As it is, however, the atmosphere reflects and refracts sunlight so that the light reaching a module is composed of 'direct' and 'diffuse' components. The direct component is subdued by gases and particles

in the atmosphere, whereas the diffuse component comes from all over the sky and ground.

If the direct and diffuse components of irradiance are known separately, 'transposition models' need to be used to to estimate how much of it lights the flat surface of the PV module. Gueymard (2009) presents the conventional geometric model:

$$E_{\text{surface}} = E_{\text{DNI}} \cos\theta + E_{\text{diffuse}} \left(\frac{1 + \cos s}{2} \right) + \rho E_{\text{global}} \left(\frac{1 - \cos s}{2} \right) \quad (2.3)$$

where E_{DNI} is the direct incidence on a hypothetical plane normal to the sun's rays, θ is the angle of incidence of the rays on the actual surface, s is the angle of tilt of the surface from horizontal, and ρ is the ground's albedo or reflective ability. E_{global} refers to total irradiance on a horizontal plane;

$$E_{\text{global}} = E_{\text{DNI}} \cos Z + E_{\text{diffuse}}$$

where Z is the zenith angle.

The parenthesised terms in Equation (2.3) are isotropic; $(1 + \cos s)/2$ assumes uniform light from all over the sky and $(1 - \cos s)/2$ assumes uniform reflection from the ground all around. The simplicity of these assumptions introduces errors (which err on the conservative side), and better models can be used.

It may be possible to measure the direct and diffuse components separately for a location, but in practice usually only the global irradiance is known because less sophisticated measuring equipment is used. The proportion of the global irradiance that is diffuse is then estimated, which is highly inaccurate. In fact the severity of error caused by estimating a diffuse proportion outweighs by far the error caused by the transposition model. The proportion of diffuse irradiance is determined by the 'turbidity', that is the amount of aerosols in the air.

Another source of error is the estimation of the ground's albedo ρ. This is the extent to which the ground reflects light. It varies considerably depending on the type of soil or ground cover in a location, but also varies throughout the day. The extreme case is that of snow melting, which reduces albedo as it melts, but even dry ground varies throughout the day.

Methods for estimating the proportion of diffuse irradiance are reviewed by Gueymard (2009). For example, a simple correlation is provided by Erbs *et al.* (1982) for the monthly diffuse fraction which only uses the monthly average 'clearness index' $\overline{K_t}$:

$$\frac{\overline{E}_{\text{diffuse}}}{\overline{E}_{\text{global}}} = 1.317 - 3.023\overline{K_t} + 3.372\overline{K_t}^2 - 1.769\overline{K_t}^3 \ .$$

(The clearness index is the ratio of global irradiance on a horizontal surface to extraterrestrial irradiance on a horizontal surface. It is a measure of how much the atmosphere attenuates light from the sun, and can be obtained from satellite imagery.) Erbs *et al.* also give correlations for daily and hourly diffuse fractions. It should be remembered that these estimates are not very reliable.

Efficiency prediction

The easiest prediction which needs to be made for a-Si modules is that their efficiency will drop by about 20 % due to photodegradation in the first 1000 hours of 1 sun irradiance (Shah *et al.*, 2004). Apart from that, efficiency mainly varies depending on the spectrum of the incident light and the temperature.

With regards to the spectrum, it is more blue when the sun is higher in the sky, as well as when it is overcast. A blue-shifted spectrum means the optimum bandgap is higher; which favours a-Si over μc-Si or c-Si. This effect causes a fairly dramatic improvement of I_{SC} for a-Si cells at lower latitudes (Gottschalg *et al.*, 2004).

With regards to temperature, the efficiency of a-Si cells decreases as temperature increases. The effect is well-understood and represented in Equation (2.2); but uncertainty exists in predicting the actual cell temperature when the atmospheric temperature is known. Usually the cell temperature is significantly higher than the surroundings.

One method to estimate the cell operating efficiency uses the nominal operating cell temperature (NOCT). The method works as follows (Skoplaki & Palyvos, 2009). The PV cell is operated at nominal terrestrial environment conditions [not STC]. Its internal temperature is measured in these conditions with no load attached: this is called T_{NOCT}. The corresponding irradiance is E_{NOCT}. Then, when the cell is in real operation at some other ambient temperature T_{a}, its efficiency can be estimated with

$$\eta = \eta_{\mathrm{STC}} \left\{ 1 - \beta \left[T_{\mathrm{a}} - T_{\mathrm{STC}} + (T_{\mathrm{NOCT}} - T_{\mathrm{a}}) \frac{E_{\mathrm{a}}}{E_{\mathrm{NOCT}}} \right] \right\} \ .$$

Another effect of temperature in a-Si cells is thermal annealing above about 65 °C, which improves the efficiency. It is very difficult to predict the results of this. Annealing does not fix all microscopic structural faults; for example the contact resistance R_{S} (Gordijn *et al.*, 2006).

Instead of trying to predict the several effects of spectrum and temperature on the efficiency of a cell, it can be easier to use empirical studies by others. Recorded results show the combined effects of temperature including annealing and the change of light spectrum in summer. They do not necessarily apply to different locations, however. An example recorded by Adelstein & Sekulic (2005) at a 40° latitude showed 10.5 % higher efficiency in summer.

Algorithms

The methods for estimating weather and the resulting power output can be divided into three conceptual categories: the typical meteorological year, compressed weather data, and analytical averages. All methods use the clearness index to some extent as an indicator of irradiance levels.

Typical meteorological year The typical meteorological year (TMY) is a brute force technique which takes the expected irradiance, expected efficiency due to temperature, and the panel orientation. The power output is calculated for each hour of each day for a whole year and summed to give the total output. The typical weather data used for the year are averaged from long-term measurements.

This method requires hourly irradiance data (or alternatively, K_t data), hourly temperature data and a lot of computing time. The PV-DesignPro computer simulation used in this project, discussed in Appendix B, made use of the TMY method.

Compressed weather data Another method presented by Celik (2003) uses a short compressed 3 or 4 day month with synthetic weather data. The synthetic data can also be derived from clearness index data. A frequency distribution of daily K_t values in a specific month is used to choose the representative K_t values for each of the days. The hourly irradiance data are then synthesised — this step only requires the hour of sunset or sunrise in the month.

After the synthetic data have been produced, the method effectively follows the same approach as the TMY method. The synthesised irradiance, the corresponding estimated efficiency and the panel orientation are used to calculate power outputs for every hour in each compressed month, which are then summed.

The advantage of the compressed weather data method is that it is much quicker than the TMY method and still fairly accurate. The method requires monthly $\overline{K_t}$ data as well as the frequency distribution of K_t for each month.

Analytical average Monthly average irradiance and monthly average efficiency can be determined using analytical integrations if perfect data are known. Gong & Kulkarni (2005) present empirical relations which approximate these analytical integrations, using only $\overline{K_t}$. The energy output for each month can then be estimated using the average irradiances and efficiencies.

This method only requires monthly average $\overline{K_t}$ values.

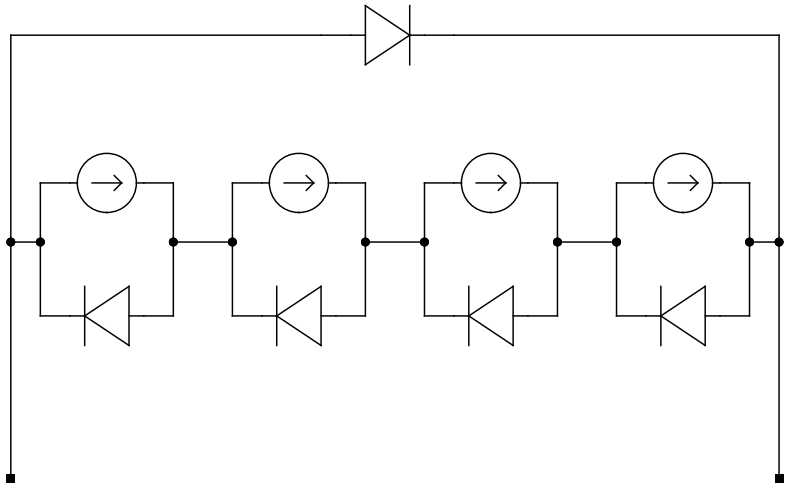

Figure 2.3: Bypass diode connected over a series string of PV cells

2.6.2 Shading

PV cells need to be connected in series to increase the voltage and reduce the current, since each cell supplies a small voltage of about 0.5 V to 1 V. When large arrays are created there are usually several parallel strings, though, to prevent the voltage becoming unmanageably large. These interconnections between cells need to be designed to provide modularity to cope with shading and failure of cells.

Bypass diodes

When a shadow is cast over a PV cell its current output drops dramatically; to 0–10 % of full output. For cells in series, this limits the current of the whole string. If the other cells in the string are unshaded they generate a reverse voltage drop over the shaded cell, which may cause it to operate in reverse breakdown. Operating in reverse breakdown damages PV cells permanently, especially because they dissipate large amounts of power as heat. The heat can also burn out connections and the encapsulation.

The solution to shading-induced breakdown is to connect a bypass diode over a short string of cells, as shown in Figure 2.3. When one cell is not operating (modelled by removing its current source), the reverse voltage over it is limited to the sum of voltages of the other cells plus the drop over the bypass diode.

Conventionally bypass diodes have only been used to prevent reverse breakdown (Woyte *et al.*, 2003) despite their usefulness for modularity. It can be

seen that each bypass diode creates an independent module out of its series string. A cell that fails will only render ineffective the other cells that are covered by the same bypass diode, not further cells. This suggests that more bypass diodes would make an array more robust and allow it to operate proportionally when partially shaded. More are not used, however, and usual designs only incorporate a bare minimum of bypass diodes; about one per 18 series cells. A reason often cited for having few bypass diodes is aesthetic appeal, and perhaps cost saving is also a factor.

Having a long string of cells that becomes ineffective all at once means a severe loss of power, disproportionate to the level of shading. It also causes the maximum power point (MPP) to move and makes it difficult to track effectively (Silvestre *et al.*, 2009).

The natural conclusion is that more bypass diodes are better. They are of negligible cost compared to the PV cells they protect. It might even be possible to incorporate them onto the silicon wafer or film (Woyte *et al.*, 2003), eliminating the dubious claim of aesthetics. Refer to Appendix A for simulation-based evidence for the benefit of many bypass diodes.

Blocking diodes

A little reflection suggests the configuration in Figure 2.4, where each series string has a blocking diode in its parallel connection with other strings. The blocking diodes would prevent a shaded string from drawing current from the other strings, but would effectively switch it off. This would ensure a maximum power output even with a string shaded.

The weakness of this design is the voltage drop over the blocking diodes. Combined with the significant current generated, a significant amount of power would be dissipated in the bypass diodes. The idea was proposed to use Schottky diodes which have low operating voltage drops, but these diodes have very high series resistances which defeat the object. (Schottky diodes are designed for low-current applications.) Blocking diodes are thus not recommended.

2.6.3 Energy storage

As with most renewable electricity, energy storage is not a natural part of PV power. Usually batteries are used to store energy on location for short-term use. Most commonly used are the relatively inexpensive lead-acid batteries. However, their cost is still significant and they have short lifetimes. The batteries often need to be replaced before the PV modules. It helps to have special electronic charge controllers to regulate the batteries' charge.

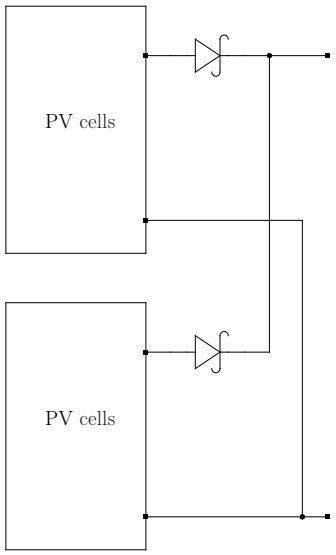

Figure 2.4: Suggested (but inappropriate) blocking diodes

An alternative to battery storage in many countries is grid connection. When power is not available from the sun it may be drawn from the conventional grid, and when excess power is available it may be sold to the grid to recuperate costs. Grid feed-in is not yet legal in South Africa. Even if it were, it would not be economically feasible without a feed-in tariff for small-scale PV or at least nett metering. (See Section 5 for one estimate of the high cost of electricity from a PV system.)

2.7 Photovoltaic roofing

A specialised application of photovoltaics is building integrated photovoltaics (BIPV), and roofing is one way to integrate PV into buildings. BIPV refers to combining the PV structures to perform other functions of the building structure, as opposed to installing extra structures purely to house PV panels. Some of the functions that can be performed well are shading and cooling, window tinting, and covering roofs and façades that are exposed to the sun. BIPV saves building materials and performs a sheltering function simultaneously with a power generating function, which leads to some stringent requirements.

2.7.1 Desired characteristics

There are some desired characteristics for PV roofing (Bahaj, 2003). It should *easily be incorporated* into the building, effectively performing the functions

Table 2.1: Three types of PV roofing and their match to the desired characteristics

Type	Ease of incorporation	Building regulations	Roofer	Electrical connections	Easy maintenance
Sheet	Very easy	Not applicable	Any person	Simple but exposed	Easy and accessible
Large tile	Difficult	Applicable	Specialised person	Few	Complicated
Small tile	Easy	Applicable	Traditional roofer	Many	Varies; usually complicated

of other roofing materials. Particularly, it should meet the relevant *building regulations* for the normal materials. It should be possible to install by a *traditional roofer* in approximately the same time as a traditional roof. As part of this, it should use *standard electrical connections* that are not unnecessarily complicated. This should also apply to future work and there should be an *easy route for maintenance*.

2.7.2 Types of photovoltaic roofing

Three forms of PV roofing are commonly encountered. Long sheets are made for laying out on the existing roofing; some examples are produced by UniSolar and Alwitra. Large tiles are made to replace a number of conventional tiles each; some examples are produced by General Electric Solar, OkSolar, Rheinzink, SolarCentury and SunPower. Small tiles or 'shingles' are made to replace a single conventional tile each; some examples are produced by Solardachstein and Sunslates. (The KissTile was another experimental tile that also incorporated water heating.) The smaller sort of tile is the concept investigated by this project.

The three types of roofing are compared in Table 2.1 for how well they match up to the desired characteristics above.

SunSlates small tiles are installed at the Sustainability Institute in Stellenbosch, and they illustrate a number of design mistakes (Rautenbach, 2008). Each tile has 6 crystalline silicon cells and delivers 14 W at 3.7 V. The tiles are connected in series strings without regular bypass diodes. The tiles are tightly nailed and wired to the roof. In addition, tiles overlap the ones below them tightly. It is actually necessary to remove a V-shape of all the tiles above a particular tile before it can be removed. This makes replacement of a faulty PV tile quite laborious.

The weaknesses of the SunSlates tiles are the following. As their first weakness, the PV cells are not integrated into the tiles but stuck on in a separate manufacturing process. This adds extra expense and weight. As their second weakness, the tiles are so heavy that extra roofing framework needs to be built to support them. As their third weakness, their omission of bypass diodes means a single failure disables the whole array. As their fourth weakness, the tiles are very difficult to replace.

The concept introduced by this project has learnt from the weaknesses of the SunSlates tiles and meets all Bahaj's desired characteristics for PV roofing listed above. Replacing the conventional concrete roof tiles means they will be loose-fitting and easy to install or remove a few at a time. This will also allow for easy electrical connections that are still protected by being located underneath the tiles. The incorporated bypass diodes mean robust operation under shadowing. Using polypropylene reinforced with glass fibres means the tiles can be strong enough to meet building regulations.

2.7.3 Weathering

Roof tiles are exposed to severe weathering conditions (Berdahl *et al.*, 2008). They may suffer UV degradation, corrosion from acidity, temperature variations, biological growth, and other attacks. Plastics and glass can be weighed up with regards to their response to weathering.

Weathering of plastics

Plastics are generally damaged by ultraviolet light. They become brittle and crack. Polyester forms a chalky layer which would obstruct light for PV applications, although it can be modified by silicone to reduce this. Polypropylene, used by the Lomold process for this project, oxidises under UV light to form C=O groups and then cracks easily.

Some plastics become brittle in cold weather, that is they lose their elasticity. The temperature ranges of plastics should be considered when they are chosen.

Some types of biological growth, such as cyanobacteria, are common on roofs and would obstruct light for PV applications.

Substances can be mixed into plastic to overcome some of the above problems. Absorbers of UV light can be incorporated, although common ones such as TiO_2 that reflect light are not suitable for PV's light absorption. It appears that PowerFilm Solar (2009) has a UV absorber that is transparent. Biocides can also be included into the plastic in warm climates where that is necessary.

Weathering of glass

Put simply, glass suffers from none of the above problems with plastics. It would be preferable for roofing with regards to weathering problems. Glass tiles have been made on an experimental level by Matsuoka *et al.* (1990) but they are apparently not in production. This may perhaps be due to the complicated manufacturing process of a-Si on curved surfaces.

2.7.4 Social impacts

Hondo *&* Baba (2009) performed a study in Japan on the effects of PV systems on families that installed them. The main result was that families with PV systems were more environmentally conscious, especially in saving energy. There was a causal relationship between the awareness of the PV system and the increase in environmentally-responsible behaviour; which suggests that the systems should preferably be highly visible. An additional contributing factor was family involvement and communication about the PV system.

The deduction relevant to this project is this: Due to their impact on other energy-related behaviour, *PV systems will save more energy than they generate.* Their importance to South Africa's current electricity crisis should thus not be underestimated.

3 Methodology

This section presents the rationale, materials and methods of the work done. For the results obtained and their interpretation, refer to Section 4.

3.1 General approach

The experimental part of this project focussed on the effects of the Lomold process on a particular type of PV cell. Firstly, the most promising PV technology was chosen. It was chosen according to how well its characteristics met the goals of the roof tile as an end product. Secondly, some sample PV modules were obtained. They were tested to determine their electrical characteristics 'out of the box'. Thirdly, the modules were moulded into plastic structures using the Lomold machine. They were then tested again to see how their electrical characteristics had changed. The results were analysed and clear conclusions were reached about the damage to the PV modules.

3.2 Chosen PV technology and module

3.2.1 Chosen technology

Amorphous silicon (a-Si) was chosen as the best PV technology for plastic roof tiles. The reasons for this were as follows.

At the highest level, it is necessary to use a thin-film technology. Thin films are flexible and not fragile, which is essential for tiles that are to be handled in bulk as building materials. Moreover, roof tiles usually have curved shapes, but both monocrystalline and multicrystalline solar cells cannot be fitted to curved shapes. Since the idea is to have tiles that fit in aesthetically with the rest of the roof, a technology is needed that can be fitted onto curved tiles after manufacture; or else be deposited onto a curved surface directly. These options are available only for thin films.

At the next level, a thin film is required that can be deployed on a huge scale in a residential context. The expense of the traditional III-V technologies rules them out, as does the experimental nature of the dye-sensitised and organic technologies. What is left are the chalcopyrites (CIGS), CdTe and a-Si. CIGS is still not widely available due to delays in scaling up its production processes. Ultimately it can never be produced on massive scales because of the shortage of indium (Grama, 2007). Either CdTe or a-Si could really be used for this project. It was decided, however, that silicon is a safer option for the residential context because the long-term health effects of CdTe are still mostly unknown. In addition, in the long term, tellurium supply could become a limiting factor whereas silicon will not.

There are additional benefits of amorphous over crystalline silicon that would give it preference even if flat roof tiles were acceptable.

1. The performance of a-Si degrades with temperature at about half the rate that the performance of c-Si does (0.26 % opposed to 0.45 %). This means that if an a-Si cell is 6 % efficient and a c-Si cell is 14 % efficient, then a temperature rise of

$$\Delta T = \frac{14 - 6}{0.45 - 0.26} = 42\,^{\circ}\mathrm{C}$$

   would make their performance equal. Temperatures like this are easily reached in practice.

2. Amorphous silicon can withstand thermal expansion and contraction without any negative effects on its efficiency.

3. Amorphous silicon cells can be connected in series monolithically on the substrate. Thus lower-current modules can be formed on small sizes such as roof tiles.

3.2.2 Chosen module

The brand of amorphous silicon chosen was PowerFilm Solar (2009). The specific product chosen was the S-PT15-150, with a total size of 170 mm × 280 mm and nominal operation at 15.4 V and 100 mA. PowerFilm was the only manufacturer found that made plastic modules in small enough sizes to be feasible for roof tiles. Some other manufacturers are listed in Table 3.1. The modules were chosen because of their size, because they are plastic and flexible, because they are suitable for original equipment manufacturers (OEMs) and because they are treated with UV absorbers.

The size of less than about 300 mm × 300 mm is important so that the roof tile can be the same size as conventional tiles. The context of this project

Table 3.1: Some manufacturers of a-Si modules

Manufacturer	Country	Smallest size [mm^2]	Flexibility	Notes
Auria	Taiwan	1300 ×1100	-	
ENN	China	1300 ×1100	-	
EPV	USA	1245 × 635	-	
Flexcell	Switzerland	695 × 350	Flexible	Partners for BIPV
ICP / SunSei	Canada	394 × 127	-	
Inventux	Germany	1300 ×1100	-	Micromorph
Kaneka	Japan	990 × 960	-	
PowerFilm	USA	270 × 100	Flexible	
Signet	USA	1300 ×1100	-	
Sunfilm	Germany	1300 ×1100	-	
UniSolar	USA	2850 × 394	Flexible	

was plastic roof tiles, for which plastic PV modules are the most suitable. Unpackaged OEM parts were needed so that they could be moulded without disassembly. Finally, UV absorbers are necessary for a plastic product that will spend much time in direct sunlight; otherwise it will become brittle and discoloured.

PowerFilm was unresponsive to requests for information on the physical characteristics of the modules; such as the tensions, temperatures and pressures that they can withstand. However, it is known that the modules are made of polyamide (nylon) — a thermoplastic well known for its toughness, abrasion resistance and high temperature limits (IDES, 2009).

3.3 Experiment for the effects of moulding

3.3.1 Aim

The aim of this experiment was to subject the a-Si modules to Lomold's injection moulding process, and to determine the nature and extent of their degradation.

3.3.2 Hypothesis

The null hypothesis was that the characteristics of the PV modules do not degrade in the moulding process. The hypothesis applied to the following characteristics:

open-circuit voltage	V_{OC},
short-circuit current	I_{SC} ,
fill factor	FF ,
lumped parallel resistance	R_P , and
lumped series resistance	R_S .

Note that it is actually expected that the characteristics do degrade: the null hypothesis was set to the opposite so that it could be disproved.

The unknown factors in the degradation process were the pressure and temperature limits of amorphous silicon. Although literature has been found on the effects of in-plane strain (Jones *et al.*, 2002), none has been found on the effects of strain perpendicular to the plane of the thin film. Similarly, although the temperatures for forming the thin film are well understood, the effects of high temperatures for short durations on a completed film are not.

Particularly, it was unknown if the effects of thermal annealing would be beneficial for such short durations of heating or under such high pressures.

3.3.3 Approach to the experiment

The experimental results were based on the electrical characteristics of the PV modules before and after moulding. Firstly, the current-voltage (I-V) curves were tested under artificial light conditions. Next, the modules were moulded into a generic mould using the Lomold machine. Thirdly, the I-V curves were again tested under the same artificial light conditions. Finally, the curves were compared to see what changes had occurred.

3.3.4 Experimental setup for testing I-V curves

Equipment

The following equipment was used.

- PVPM 2540C peak power measuring device and I-V curve tracer. It was manufactured by 'pve Photovoltaic Engineering', Germany. It included a temperature sensor and an intensity meter, which were calibrated under standard test conditions after manufacture.

- Personal computer with a standard RS-232 port and the 'PVPM.disp' software for data logging. The software accompanied the PVPM.
- Connector cables with crocodile clips. These were used to connect the PVPM to the PV module.
- 1000 W incandescent light bulb, with an autotransformer ('variac') to set the voltage as needed.
- Four PowerFilm PT15-150 plastic a-Si modules.

Arrangement

The bulb was hung from the wall and connected via the autotransformer to the electrical supply. While each PV module was being tested, it was placed at approximately 30° to the horizontal on a platform, about 30 cm below the light bulb. The same positioning was used for each module before moulding, but a slightly different positioning was necessary after moulding because of the bulky plastic structure.

The light meter was placed next to the PV module. It also was placed consistently before moulding and consistently in a different position (closer to the bulb) after moulding.

The light bulb was an ordinary incandescent one and did not attempt to approximate the solar spectrum. Its light was noticeably yellow and thus not ideal for the large bandgap of a-Si modules. Nevertheless, reasonably consistent light was obtained by setting the voltage supplied to the bulb.

There was some lack of precision in the experimental setup, which was not ideal. In addition to the placement difficulties above, the room was lit by fluorescent lights in addition to the 1000 W bulb, and there were windows looking outdoors. Fortunately there was not line of sight to the sun or the sky. The imprecision was later accounted for by adjusting the current readings according to the intensity measured by the light meter.

3.3.5 Test procedure for I-V curves

The PVPM's facility for automated I-V curve measurement was used. The data obtained were noisy so 10 repetitions were made of each measurement. Before each set of measurements the module was allowed at least 1 min to warm up under the heat of the light. The temperature was not fully stabilised when measurements were taken.

During the PVPM's curve measurement, the values of V_{OC} and I_{SC} were determined separately. They were used to determine the range of the rest of the voltages and currents. Then a range of non-uniform voltage increments was

applied and the current was determined at each voltage step. Only absolute voltages greater than 1 V were measured by the machine, so it was only capable of testing modules and not individual cells.

3.3.6 Moulding

Lomold (2009) has a unique and patented injection moulding process. The main difference from the normal process is that molten plastic is fed very quickly into the mould using a piston. High pressures and high temperatures are involved in this process.

The machine used for this project allows a maximum pressure-area product of about 16 tonnes. Polypropylene mixed with short glass fibres was used to reduce the shrinkage on cooling. This mixture also provides more structural rigidity. The temperature reached a maximum of about 220 °C during the process, although this was only for a short time. The PV modules were only subjected to this temperature for less than 10 s during the piston's moulding stroke.

The four PV modules were moulded in turn into flat plastic serving trays. Each module's light collection surface faced outwards, flush with the rest of the surface of the tray, and the module's reverse surface was embedded in the tray. The following points were important about the moulding of the individual modules.

Module A was moulded with too much plastic material. As a result a thick column of plastic was formed at the top of the piston's cylinder, attached to the centre of the tray. This column remained hot for several minutes after moulding and kept the centre of the PV module hot too. The mould did not fill all the way to its extremities, because the PV module filled too much of the cavity width and caused a large pressure drop.

Modules B, C and D were moulded with less plastic material. It was accepted that the mould would not fill all the way to its extremities. The tray cooled to room temperature within a minute of moulding.

3.3.7 Re-testing the I-V curves

The same setup and procedure as before were used after the moulding of the PV modules into the plastic structures. The setup and procedure are detailed in Section 3.3.4 and Section 3.3.5.

3.3.8 Processing the data

The steps used to prepare the data for comparison are presented here. Tests done before moulding will be called 'Before' tests, and those done after moulding will be called 'After' tests.

Adjustments for irradiance

As mentioned above in Section 3.3.4 the irradiance levels varied between modules on a day and between testing days. The following adjustments were made to attempt to compensate for this in the most conservative way. That is, the adjustments would err on the side of making it harder to disprove the null hypothesis.

The irradiance measured by the light meter in all the After tests was higher, surely due to the fact that the light meter was positioned closer to the bulb. Yet all the values of I_{SC} were degraded in the After tests. Thus it was assumed that the irradiation was in reality less After than Before. The *first adjustment* was this: since the smallest degradation of I_{SC} was 5 %, all the After I values were multiplied by 1/0.95. This gave the best-case scenario that Module B's I_{SC} did not degrade at all (since it was not feasible that it would have improved). Note that the bias of this adjustment was towards the null hypothesis that the modules did not degrade.

On each day the intensity of light fluctuated between measurements. The reason for this was not clear. It may simply have been due to the fluctuations in the line voltage, or due to the heating and cooling of the light bulb. The average irradiance on each module was determined. Then the *second adjustment* was this: all the I values for a module were adjusted upwards if its irradiance was less than the day's average, or adjusted downwards if its irradiance was more than the day's average. Each adjustment was a multiplication by

$$\frac{\text{Irradiation average for the day}}{\text{Irradiation average for the module for the day}} .$$

Data smoothing

The Before data conformed well to the expected shape of a photovoltaic I-V curve. Therefore it was sensible to to fit the curves to a standard single-diode model. The model used was the five-parameter implicit model for I given a value of V:

$$I = I_{\mathrm{L}} - I_{\mathrm{o}} \left[\exp\left(\frac{V + IR_{\mathrm{S}}}{nV_T} \right) - 1 \right] - \frac{V + IR_{\mathrm{S}}}{R_{\mathrm{P}}} . \tag{3.1}$$

The following simplified parameter extraction method was used as presented by de Blas *et al.* (2002).

1. $R_\mathrm{S} = 0.2\,\Omega$ and $R_\mathrm{P} = 5\,\mathrm{k}\Omega$ were chosen as typical values for a-Si cells. As Celik *&* Acikgoz (2007) discuss, the sensitivity of the model to the slopes of the graph at V_OC and I_SC is small, so by inference the sensitivity to R_S and R_P is small. This means it was acceptable to choose fixed values for them manually. The values were initially chosen with reference to Stutenbaeumer *&* Mesfin (1999) with $R_\mathrm{S} = 5\,\Omega$. However, this initial value of R_S gave a shallow slope at V_OC that did not fit the measured data well, so it was adjusted manually for a better fit.

2. The value of R_S was multiplied by 12; the number of series cells in the module.

3. The MPP was estimated by the average of five measurements. The measurements nearest the maximum measured V and I were averaged to give V_m and I_m.

4. The non-ideality factor n, the saturation current I_o and the photocurrent I_L were determined from the following formulas.

$$n = \frac{V_\mathrm{m} + I_\mathrm{m} R_\mathrm{S} - V_\mathrm{OC}}{V_T \ln\left[\dfrac{I_\mathrm{SC} - I_\mathrm{m}\,(1 + R_\mathrm{S}/R_\mathrm{P}) - V_\mathrm{m}/R_\mathrm{P}}{I_\mathrm{SC}\,(1 + R_\mathrm{S}/R_\mathrm{P}) - V_\mathrm{OC}/R_\mathrm{P}}\right]}$$

$$I_\mathrm{o} = \frac{I_\mathrm{SC}\,(1 + R_\mathrm{S}/R_\mathrm{P}) - V_\mathrm{OC}/R_\mathrm{P}}{\exp\left(\dfrac{V_\mathrm{OC}}{nV_T}\right)}$$

$$I_\mathrm{L} = I_\mathrm{o}\left[\exp\left(\frac{V_\mathrm{OC}}{nV_T}\right) - 1\right] + \frac{V_\mathrm{OC}}{R_\mathrm{P}}$$

   The temperature T was assumed as a constant of 50 °C. Note that the value obtained for n was that of the module, and should be divided by 12 to get the value for a single cell.

The model parameters were calculated for every measured I-V curve and then the parameters were averaged over the 10 measurements for each module. An arithmetic mean was used because the parameters did not vary very much, with the exception of I_o. For I_o a geometric mean was used because I_o is multiplied by an exponential term in the model, and its calculated values varied in an order-of-magnitude way.

The After data did not fit the shape of the model in Equation (3.1) at all. It was decided simply to smooth the curves by dividing them into voltage ranges

and taking the average of the current measurements in each voltage range. The voltage ranges were nonuniform for better accuracy at the higher voltages.

The difference in data smoothing method Before and After meant that the parameters of the diode model could not be compared directly. However V_{OC} and I_{SC} could be compared, as could the fill factor (FF) calculated from the MPP.

3.4 Moulding crystalline silicon cells

It was also planned to mould crystalline silicon solar cells, as a direct means of encapsulating them. However, the moulding was completely unsuccessful.

The crystalline cells were laminated to glass on one side using acid-free silicone to form half-modules. The goal was to mould these directly into plastic structures as done above for the a-Si cells.

No suitably sized proper mould was available, however, so it was attempted to use temporary poly-vinyl-chloride (PVC) moulds. The PVC could not withstand high enough pressures. Thus the mould could not be packed as the plastic cooled and shrank, so the plastic pulled back from the crystalline cells and shattered them.

4 Results and analysis

This section presents the results obtained and their interpretation. For the rationale, materials and methods of the work done, refer to Section 3.

4.1 Nominal module efficiency

The PowerFilm modules are advertised to operate at $V_{\text{nom}} = 15.4\,\text{V}$ and $I_{\text{nom}} = 100\,\text{mA}$, which should be the maximum power point (MPP) of the modules. It is not clear whether this refers to the power output after initial photodegradation, but it is assumed that the modules are designed to conform to this for standard test conditions (STC) at the time when they are bought. Thus the nominal power output is $P_{\text{nom}} = V_{\text{nom}} I_{\text{nom}} = 1.54\,\text{W}$.

Each module has an active area of

$$A = 238\,\text{mm} \times 144\,\text{mm} \approx 0.0343\,\text{m}^2 \,.$$

At STC the incident radiation is $E_{\text{STC}} = 1000\,\text{W/m}^2$, so the nominal efficiency of the modules is

$$\eta_{\text{nom}} = \frac{P_{\text{nom}}}{A E_{\text{STC}}} = 4.49\,\% \,.$$

If the estimate of Shah *et al.* (2004) is used that production modules operate at 65 % of the laboratory efficiency, then these modules correspond to a technology which achieves 6.9 % efficiency in the laboratory. This is comparable to the 7 % stabilised efficiency achieved by the Helianthos project for a double-junction a-Si cell (Rath *et al.*, 2008). The Helianthos process uses deposition on aluminium and then transfers the cell to a plastic substrate. It is less than the 8 % stabilised efficiency achieved by Fuji Electric for double-junction a-Si cells on polyimide (Tanda *et al.*, 2005). It is also less than the 8.7 % stabilised efficiency achieved by Haug *et al.* (2009) for a tandem μc-Si/a-Si cell. Haug *et al.* deposited on PET and PEN polymer substrates.

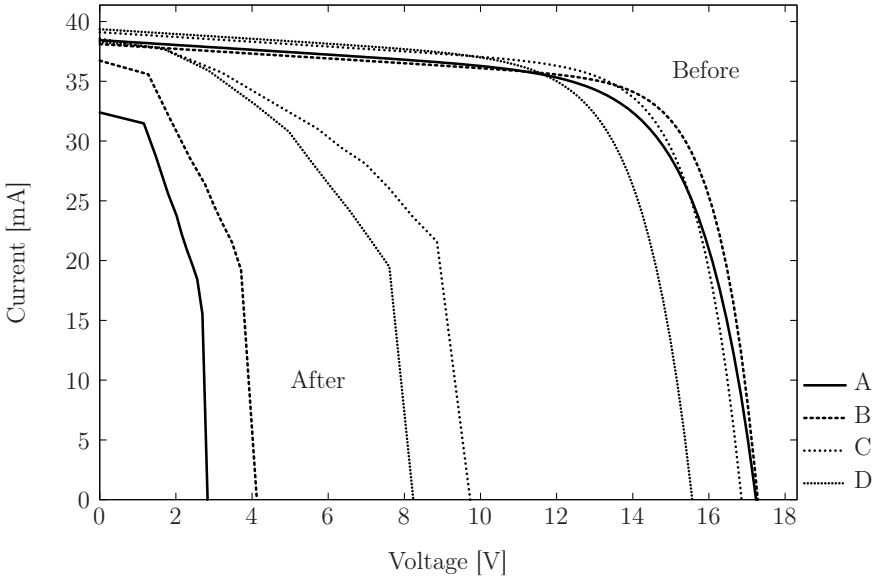

Figure 4.1: I-V curves of the modules before and after injection moulding

Table 4.1: Electrical parameters of the modules as received

Module	η [%]	V_{OC} [V]	I_{SC} [mA]	V_m [V]	I_m [mA]	FF
A	2.33	16.9	38.4	14.2	30.1	0.658
B	2.65	16.8	38.1	14.3	32.0	0.719
C	2.51	16.5	39.1	14.0	32.2	0.701
D	2.26	15.4	39.4	12.9	31.7	0.677
Mean	2.44	16.4	38.8	13.9	31.5	0.689
Standard deviation	0.18	0.70	0.58	0.66	0.97	0.027

4.2 Experiment for the effects of moulding

The I-V curves for the modules are compared in Figure 4.1. It should be remembered that the test conditions used are not standard test conditions, so the values should not be used in comparison with other literature without modification. There are a few points of note, discussed below.

4.2.1 Variation in parameters

The first observation is that there was quite a large variation in the parameters of the modules 'out of the box'. This is also evident from Table 4.1. The open-circuit voltage ranged between 15.4 V and 16.9 V, the short-circuit current ranged between 38.1 mA and 39.4 mA. The calculated fill factor ranged

between 0.66 and 0.72 and the efficiency ranged from 2.26 % to 2.65 %. A high variation in parameters for a-Si modules was also reported by Gottschalg *et al.* (2004).

This variation of parameters would be quite important when modules become connected together to form an installation — the total efficiency would be less than the sum of the modules' efficiency. Using the method proposed by Kaushika & Rai (2007), the fractional power loss expected for these $N = 4$ modules in series would be as follows.

$$\begin{aligned} C &= \frac{q\overline{V_\mathrm{m}}}{\overline{n}kT} = \frac{(1.60{\times}10^{-19}\,\mathrm{C})(13.9\,\mathrm{V})}{40.7(1.38{\times}10^{-23}\,\mathrm{J/K})(323\,\mathrm{K})} \\ &= 12.3 \end{aligned} \tag{4.1}$$

$$\begin{aligned} \mathbb{E}\left[\frac{P_\mathrm{lost}}{N\overline{V_\mathrm{m}I_\mathrm{m}}}\right] &= \frac{C+2}{2}\left(\frac{\sigma_{I_\mathrm{m}}}{\overline{I_\mathrm{m}}}\right)^2\left(1-\frac{1}{N}\right) \\ &= \frac{12.3+2}{2}\left(\frac{0.97}{31.5}\right)^2\left(1-\frac{1}{4}\right) \\ &= 5.1{\times}10^{-3} \end{aligned}$$

Thus the power lost only due to interconnection would be 0.51 % of the expected $P = N\overline{V_\mathrm{m}I_\mathrm{m}} = 1.75\,\mathrm{W}$.

4.2.2 Lower efficiency than expected

The second observation is that the efficiency of the modules was quite low at 2.4 %. This was surely due to the yellow source of light used, as yellow light gives a-Si cells a disadvantage due to their high bandgap. The low light intensity would also have had a minor effect because the voltage decreases logarithmically with light intensity.

4.2.3 Degradation proportional to heating time

The third observation is that some modules degraded far more than others. In particular, Module A's efficiency degraded to 12 % of its original value, as can be seen by comparing Table 4.2 to Table 4.1. The resulting efficiencies of the other modules were also heavily degraded, but not as much. Individual graphs show this clearly in Figure 4.2. There was a correlation between the length of time that the modules were hot and the extent of their degradation.

This suggests that the temperature of 220 °C is too high for the amorphous silicon to retain its structure and properties, but also that the degradation took place gradually over a time period measurable in seconds. The moulding

Table 4.2: Electrical parameters of the modules after moulding

Module	η [%]	V_{OC} [V]	I_{SC} [mA]	V_m [V]	I_m [mA]	FF
A	0.28	2.8	32.4	2.3	21.6	0.552
B	0.44	4.1	36.7	3.6	21.4	0.510
C	1.18	9.7	38.6	8.0	25.5	0.546
D	0.89	8.2	38.3	6.5	25.6	0.526
Mean	0.70	6.2	36.5	5.1	23.5	0.534
Standard deviation	0.41	3.3	2.9	2.6	2.4	0.019

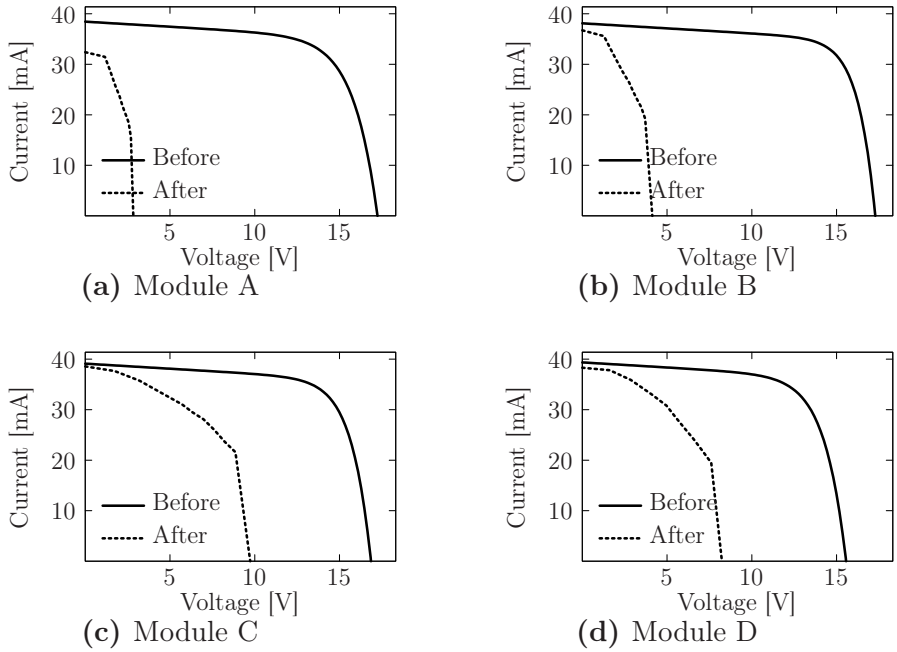

Figure 4.2: Degradation of the individual I-V curves due to injection moulding

temperature was of the same order as the temperature of the substrate during deposition of the thin film, so it makes sense that the structure was unstable at that temperature. Thermal annealing did not have a beneficial effect, which was attributed to the very high pressures to which the thin films were subjected.

To solve the problem of the degradation it would be necessary either to reduce the moulding temperature or to reduce the time that the PV module is kept hot. It would be more feasible to cool it quickly after moulding. Fast cooling of the moulded product needs to be an essential part of the production process for a-Si photovoltaic roof tiles.

The fast moulding process used by Lomold should be capable of this kind of

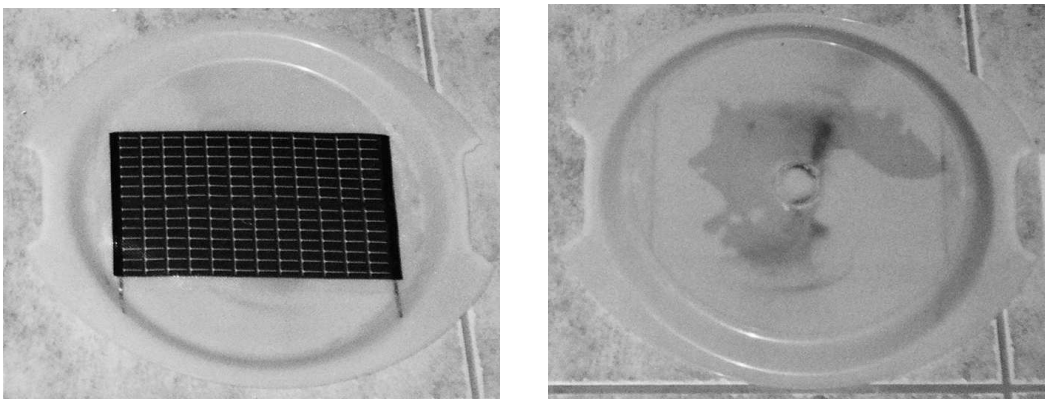

(a) (b)

Figure 4.3: Module D moulded into a plastic tray: (a) front view and (b) back view

modification. A very important point is that *conventional injection moulding would not be suitable* for incorporating a-Si photovoltaic modules.

4.2.4 Delamination

Immediately after moulding the PV modules started to delaminate from the trays they were moulded into. This should have been expected because the modules were encapsulated in polyimide, but the trays were made from polypropylene. A photograph of the reverse of one of the trays shows the delamination in Figure 4.3. The lighter patches show where the module is not bonded to the tray.

Another reason which contributed to the immediate delamination was compressive stress. The trays shrank as they cooled. Even though the shrinking was less than it would have been without glass fibres, it was still significant: the modules became warped and lifted off the flat surfaces of the trays in what looked like bubbles.

A possible solution to the problem of delamination would be to use an EVA sheet as a glue between the module and the tray. The moulding temperature would be high enough to activate it. In addition, it would remain quite liquid and fill gaps due to shrinking until the tray cooled below about 70 °C. [This is the melting temperature of EVA. After curing by exposure to light in combination with a curing agent, its melting temperature becomes much higher (Czanderna & Pern, 1996).] A good bond would be achieved by co-extruding the EVA layer with the polyamide backing of the module, but this would make long transportation of the module before moulding infeasible.

5 Economic viability in the Western Cape

A fictional housing project was analysed to determine the price of electricity from photovoltaic roof tiles. The project was situated in Oudtshoorn in the Western Cape, in the open area north of Voortrekker street in Figure 5.1. [The chosen location was largely for the sake of argument, although a large housing project has been planned for Oudtshoorn since 2004 (South African Government, 2004).] The project was arbitrarily assigned to consist of 500 houses. The houses would be freestanding, as is the trend in South African

Figure 5.1: Aerial view of Oudtshoorn showing the open area for the housing project (Google Earth, 2009)

housing developments. It was also assumed that the area had no previous access to electricity.

The viewpoint taken was that of a developer seeking to build the housing project. The developer had the option either (a) to install a PV rooftop for each house, or (b) to connect the houses to the national grid. If the houses were provided with PV systems, they would be billed by the developer for their electricity used. (It was assumed that the PV cells would be working properly after manufacture, unlike the ones moulded so far.) If the houses were connected to the grid, they would buy electricity from Eskom through the developer. The developer would add a margin to the electricity price. Either way the developer would aim to recover costs by using the electricity tariff.

The question to be answered by this analysis for both options, then, was this:

> What price would the users have to pay for electricity to cover the development costs specifically for electricity?

The price was expressed in '2010 rands', that is at the current value of the currency. A 15 % nominal minimum acceptable rate of return per year was assumed, so future money was discounted at this rate.

There would be many costs involved in such a project, but most of them would be common to the two options chosen. Thus only relevant costs were considered. These were the costs unique to a specific option; either PV roofing or grid connection.

Note that this analysis would still hold if the developer were the municipality, as long as a modification was made. The electricity tariffs from Eskom would have to be modified because they are higher for municipalities than for businesses.

5.1 PV option

The first option available to the developer was to install plastic photovoltaic roof tiles and the accompanying systems on each house.

5.1.1 Number of tiles

It was assumed that each house would need about 4 kWh energy per day. The climate in the Western Cape can be expected to provide an average of 4 kWh

per peak kilowatt of solar panels per day (Huld *et al.*, 2005). About 1 $\mathrm{kW_{pk}}$ of panels would therefore be appropriate per house.

Extra tiles would be needed, however, due to the series and parallel connection losses caused by the variations in V_m and I_m. The total number of tiles was denoted by N. They would be laid out as N_P parallel strings of N_S each, so that $N = N_\mathrm{P} N_\mathrm{S}$. Since the maximum inverter input voltage is generally 48 V, only four tiles would be laid in series ($N_\mathrm{S} = 4$). A large number of parallel strings would then be needed, which for the mismatch losses was considered infinite ($N_\mathrm{P} \to \infty$). Referring to Table 4.1, Equation (4.1) and Kaushika & Rai (2007), the following fractional loss could be expected:

$$\begin{aligned}\mathbb{E}\left[\frac{\Delta P}{P}\right] &= \frac{C+2}{2}\left\{\left(\frac{\sigma_{I_\mathrm{m}}}{I_\mathrm{m}}\right)^2\left(1-\frac{1}{N}\right) - \left[\left(\frac{\sigma_{I_\mathrm{m}}}{I_\mathrm{m}}\right)^2 - \left(\frac{\sigma_{V_\mathrm{m}}}{V_\mathrm{m}}\right)^2\right]\frac{N_\mathrm{P}-1}{N}\right\} \\ &= \frac{12.3+2}{2}\left\{\left(\frac{0.97}{31.5}\right)^2(1) - \left[\left(\frac{0.97}{31.5}\right)^2 - \left(\frac{0.66}{13.9}\right)^2\right]\left(\frac{1}{4}\right)\right\} \\ &= 0.91\,\% \,.\end{aligned} \tag{5.1}$$

The mismatch connection losses would thus be quite small. The appropriate number of 1.54 W tiles to provide 1 $\mathrm{kW_{pk}}$ would be

$$N = \frac{1000}{1.54(1-0.0091)} \approx 656 \qquad \text{(a multiple of } N_\mathrm{S}\text{)}.$$

5.1.2 Cost of the tiles

The cost of a single tile was calculated as in Table 5.1. The cost of a single PV module was 46 USD to OEMs, which translated to R 368 at an exchange rate of 8 R/USD. The initial cost of a die for the mould was approximately R 50 000 (Louw, 2009). This was averaged over all the tiles for the 500 houses, which gave the figure in the table. It is clear that the cost of the PV module dominated the cost of the tile. The clearest way to reduce the cost of the tile would be to find a module manufacturer that could make such small modules at better prices.

5.1.3 Cost of the photovoltaic system

A photovoltaic array would not be very useful by itself, and supporting equipment would be needed for every house. This equipment is listed in Table 5.2

Table 5.1: Calculating the cost of a PV tile

Item	Details	Cost [R]
PowerFilm PV module	15.4 V, 0.100 A	368.00
Polypropylene with glass fibres		10.00
EVA sheet		10.00
Die cost	Averaged	0.15
Total		388.15

Table 5.2: Calculating the cost of a PV system

Quantity	Item	Details	Unit cost [R]	Cost [R]
656	Tiles	15.4 V, 0.100 A	388.15	254 628.00
8	Batteries	6 V, 420 Ah	4 000.00	32 000.00
1	Inverter and charger	1.1 kW off-grid	20 000.00	20 000.00
1	MPP tracker		5 000.00	5 000.00
1	Billing meter		1 000.00	1 000.00
	Total			312 628.00

along with the PV tiles. The prices shown are current market prices (Sunflare, 2009). It is still clear that the cost of the PV modules dominated the cost of the system.

The total cost for all 500 houses would be about R 160 million.

5.1.4 CDM earnings

If the project were to install solar panels instead of grid connections then an amount of carbon dioxide (CO_2) would be prevented from being emitted. This is because South Africa's power stations emit a lot of CO_2 but PV panels do not. The CO_2 emissions avoided would have a value on the European Union (EU) market. EU companies who emit beyond their allowed limits may want to buy credits so that their nominal emissions may be reduced.

In fact, during their life cycle PV panels do emit CO_2. However, it was assumed that the emissions would be negligible because (a) thin films on plastic take little energy to manufacture; and (b) the tiles would replace concrete tiles. Concrete is a significant emitter of CO_2.

The amount of CO_2 saved by the PV installations was calculated. The program PV-DesignPro was used to estimate the amount of electricity that would be generated by a house's system in one year. The details of the simulation are

given in Appendix B. The result was 1400 kWh. Eskom currently produces 1.03 kg CO_2 per kWh sold (Eskom, 2009*a*). Thus a total amount of

$$(1400\,\text{kWh/house})(500\,\text{houses})(1.03\,\text{kg/kWh}) \approx 700\,000\,\text{kg}$$

carbon dioxide would be saved by the entire housing project in one year.

The economic value of that CO_2 was calculated with the assumption that a contract would be made with a European company to buy the Clean Development Mechanism (CDM) credits generated. The market price for CO_2 on the EU market was taken as 14.54 € per tonne, which was the value of the EUA OTC price on 3 November 2009. The exchange rate was taken as constant at 11.50 R/€. This was just more than an average of the exchange rates between April and October 2009 (X-Rates.com, 2009). If the CDM credits were sold each year as they were generated, but at a price fixed initially by the contract, the resulting income per year would be

$$(700\,\text{t})(14.54\,€/\text{t})(11.50\,\text{R}/€) = \text{R}\,120\,000\ .$$

The net present value (NPV) of this income over 20 years would be R 0.73 million. It would be negligible compared to the initial project costs of R 160 million.

5.1.5 Cost of photovoltaic electricity

The final cost of all the PV systems would then be about R 160 million, and the systems would generate a total of 680 000 kWh/year for 20 years. The price of electricity would thus be

$$c_{\text{PV}} = \frac{160\,000\,000}{680\,000(20)} = \text{R}\,11/\text{kWh}\ .$$

5.2 Grid option

The second option available to the developer was to connect each house to the national electrical grid. The connections would require installing a distribution line to the project location.

The grid option was perhaps not very realistic as things currently stand. Eskom has a severe shortage of peak-time capacity and is refusing new connections to large industry (Fath, 2009). Eskom is generally unwilling to add new connections that will draw power during peak times, which residential connections do.

Table 5.3: Calculating the cost of a grid-based system

Quantity	Item	Details	Unit cost [R]	Cost [R]
656	Tiles	Double Roman	7.09	4 651.04
1	Connection line		No charge	
1	Billing meter		No charge	
	Total			4 651.04

5.2.1 Cost of the grid-connected system

The costs of connecting to the grid would consist of the electrical connection costs and the ordinary tiles that would take the place of the PV tiles above. These costs are shown in Table 5.3 for a single house, adding up to about R 4700. It was assumed that the houses would be connected with the 'HomeLight 1' pricing scheme, which has been designed for small residential electricity consumers. Eskom would not charge for the connection line and the billing meter, and their costs would be absorbed into the electricity tariffs. The roof tiles used would be standard concrete, patterned tiles that fit together loosely by overlapping one another. Their price was quoted by Builders Trade Depot (2009).

5.2.2 Cost of the distribution line

Apart from the cost for each house, there would be a single cost for installing a distribution line to the housing project. The following relevant costs were obtained as fair estimates from Smit (2009).

The line planned would be about 6 km to reach from the nearest Eskom line to the project location. The required electricity supply would be considered small at 500 kW so the Fox type of distribution line would be chosen. It would match the general Oudtshoorn grid by being an 11 kV line.

The Fox lines have a rated capacity of 10.5 MW·km for a voltage drop from 104 % of optimum to 95 % of optimum. Since the planned line would extend from a non-central location on the grid, it was assumed that its voltage on the grid side would be about 100 %. Thus the line would have a reduced capacity of

$$\left(\frac{100-95}{104-95}\right)(10.5\,\text{MW·km}) \approx 6\,\text{MW·km}$$

for a voltage drop to 95 % of optimum. This would be more than enough for the 0.5 MW project at a distance of 6 km, though.

Table 5.4: Calculating the cost of the distribution infrastructure

Quantity	Item	Details	Unit cost [R]	Cost [R]
6 km	Distribution line	Fox type, short distance	250 000.00	1 500 000.00
1	Fuse	At grid side	5 000.00	5 000.00
1	Minisub	500 kVA at location	105 000.00	105 000.00
	Total			1 610 000.00

The estimated distribution costs are summarised in Table 5.4, adding up to about R 1.6 million. The cost of Fox lines is currently about R 200 000 to R 250 000 per km, with smaller projects having higher costs per kilometre. A fuse with a fairly small cost would be required at the connection to the larger grid. A 500 kVA transformer 'minisub' would be required at the project side, costing between R 80 000 and R 130 000 depending on its special requirements.

The total initial electrical costs for the project, for all 500 houses, would thus be R $[4700(500) + 1\,600\,000]$ = R 4.0 million.

5.2.3 Electricity tariffs

Although the initial cost of the grid-connected option would be less, users would pay for electricity as it was used. It was assumed that each house would consume a full 4 kWh per day, resulting in 730 000 kWh per year for the project.

The tariff in the HomeLight 1 pricing scheme was set at R 0.6778/kWh for 2010, but Eskom has planned to increase it by 45 % for three years (Eskom, 2009*c*; Maroga, 2009). The increases after that are currently unknown, but they were assumed to continue to some extent. The oil peak may affect other fossil fuel prices, the environmental levy for CO_2 will grow and Eskom's build programme will continue. The price was thus assumed to increase by 20 % per year from 2013 to 2020, and thereafter by 12 % as the build programme returned to normal.

The tariffs and resulting costs for the project over 20 years are shown in Table 5.5. The NPV would be R 22 million.

Cost of grid-based electricity

The total NPV of the grid-connected systems would then add up to about R 4.0 million + R 22 million = R 26 million, and the systems would provide a

Table 5.5: Costs of grid-based electricity over 20 years at 730 000 kWh per year

Year	Increase on previous [%]	Cost per kWh [R]	Cost for the year [R]
2011		0.98	717451.30
2012	45	1.43	1 040 304.39
2013	45	2.07	1 508 441.36
2014	20	2.48	1 810 129.63
2015	20	2.98	2 172 155.56
2016	20	3.57	2 606 586.67
2017	20	4.28	3 127 904.00
2018	20	5.14	3 753 484.80
2019	20	6.17	4 504 181.76
2020	20	7.40	5 405 018.11
2021	12	8.29	6 053 620.29
2022	12	9.29	6 780 054.72
2023	12	10.40	7 593 661.29
2024	12	11.65	8 504 900.64
2025	12	13.05	9 525 488.72
2026	12	14.61	10 668 547.36
2027	12	16.37	11 948 773.05
2028	12	18.33	13 382 625.81
2029	12	20.53	14 988 540.91
2030	12	23.00	16 787 165.82

total of 730 000 kWh per year for 20 years. The price of electricity would thus be

$$c_{\text{grid}} = \frac{26\,000\,000}{730\,000(20)} = \text{R}\,1.8/\text{kWh}\ .$$

5.3 Unquantified benefits

The result of this analysis was not complete because it neglected some other benefits of the PV systems that were hard to quantify. At least two benefits would be avoided costs to the state, that would normally be felt by other citizens as well as the electricity users.

The first avoided cost would be Eskom's cross-subsidy of the HomeLight tariff. The value of the subsidy has not been released by Eskom, but it is likely to be substantial.

The second avoided cost would be due to the health risks of paraffin and other traditional energy sources. These risks are burns, indoor pollution and poisoning from ingestion. Spalding-Fecher (2005) calculates the avoided healthcare

costs due to new electrification to be R 0.59/kWh (in 2001 rands), which is comparable to the cost of the electricity. However, this calculation includes those people who start to use electricity for cooking and so reduce their use of paraffin and wood. It is not feasible to use PV electricity for cooking, so PV electricity would not have as large a benefit as grid-based electricity in this respect.

Although PV electricity would not be useful for cooking, it would still provide some benefit of reduced indoor air pollution and reduced burns by replacing paraffin lamps. It would also provide better lighting, that could improve education prospects, and would provide access to communication that helps to inform people, such as radio and television (Spalding-Fecher, 2005).

The third benefit, which has been mentioned before, would be the renewable and distributed nature of the technology. The use of renewable power sources would help to secure a community for the future and reduce their emissions of carbon dioxide or other wastes. Distributed power generation would make the community robust against failures of the grid or of power stations.

It would be important, however, for PV technology to be deployed along with other technologies since it would not be appropriate for every end use. For example, solar water heaters would serve their purpose more efficiently, and biogas digesters or community woodlots would provide appropriate cooking fuel.

5.4 Comparing the two options

The electricity from the roof tile PV systems would cost about R 11/kWh but that bought from the grid would cost about R 1.8/kWh. The PV electricity would be an order of magnitude more expensive, when neglecting grid subsidies for the HomeLight tariffs.

It was helpful to try to determine which price of the roof tiles would make the PV electricity cost the same as the grid-based electricity. It turned out that even if the tiles had no cost the grid-based electricity would be cheaper. This unfortunate result was because of the high cost of the rest of the PV system, such as the batteries and inverter.

It was concluded that with the current state of affairs, even a PV system integrated into the roof would not compete *economically* with electricity from the grid. However, there would be other benefits such as sustainable development and reduction of health risks. These, combined with with the financial difficulties and capacity shortfall of Eskom, support the feasibility of new PV developments.

6 Considerations for manufacture

A plan to bring photovoltaic roof tiles into production needs to take into account a few important design factors. The physical strength and durability must be ensured, safe materials must be used and electrical connections and maintenance should be kept easy.

The most basic requirement is that the tiles need to be the same shape as normal concrete tiles used on South African roofs. Alternatively they could be shaped to replace the much bigger metal ('corrugated iron') tiles. Concrete tiles come in various shapes but they are typically about 35 cm × 35 cm in size with an exposed area of about 30 cm × 30 cm.

6.1 Mechanical characteristics

For tiles to be trusted in the South African market they need to comply with the relevant SABS standards. Some standards and their relevant mechanical requirements are listed in Table 6.1. Both concrete and clay tiles need holes in them for fixing to the roof trusses, which is pertinent because the tiles have such a small area and also need space for the PV modules. The Marseilles shape for clay tiles is not appropriate for light collection on a PV module because it is concave. The substance (plastic) used for the body of the tile needs to be fairly strong, and that is why it is good to include glass fibres in it.

Metal tiles are appealing because of their large size which would bring down the cost of a-Si modules. This makes products like UniSolar's stainless steel modules seem attractive. However, metal is a complex material and it needs to meet many requirements to be used on rooftops. The metal roofing standard describes how the surface needs to withstand impacts, especially hail, and thermal expansion. This is particularly relevant to PV layers on top of the main roofing material.

These mechanical requirements, in combination with the other weathering described by Berdahl *et al.* (2008) — see Section 2.7.3 — suggest that a glass covering surface is still the best choice for modules exposed to the weather.

Table 6.1: SABS standards relevant to the manufacture of PV roof tiles

Characteristic	*Required value*
SANS 542: Concrete roofing tiles	
Breaking strength	5 N/mm-of-width
Fixing holes (for wire or nails)	
SANS 632: Clay roofing tiles	
Breaking strength	6 N/mm-of-width
Fixing holes	
SANS 1022: Metal roofing tiles	
Hail resistance	10 J; 45 mm hailstone
Profile strength	800 N for 15 s
Impact resistance	5.65 J
Flexibility of coatings	25 mm radius of curvature in 1 s
Corrosion resistance	

6.2 Choice of materials

The type of polymer used in the tiles is important for durability and for human health. Especially important for durability is the mix of EVA used, as explained by Czanderna & Pern (1996). It must incorporate the right mix of UV stabilisers. An alternative to EVA that is less susceptible to UV degradation would be even better, though.

Since the tiles will be used in a residential environment they should be nontoxic. This should include non-toxicity of their fumes when they burn.

6.3 Interconnection and maintenance

Roofs often need maintenance and the addition of complex electrical systems will increase this need. The tiles should therefore be designed to be removed easily.

A very bad example to follow would be the design of the SunSlates PV tiles described in Section 2.7.2. By contrast, tiles should fit loosely with their neighbours (that is, have variable overlaps). Only the tiles at the ends of the rows should need to be wired or nailed to the roof so that any of the others can be removed at random. This may require an artificial roughness to be added to the surfaces of the tiles where they overlap so that there is more friction.

An additional reason to have a variable overlap of the tiles is so that they can easily be added to existing roofs, on which tiles are often not laid very uniformly.

The electrical connections should be located underneath the tiles so that they are protected from moisture. (Loosely fitting tiles can fairly easily be connected and disconnected electrically.)

At least one bypass diode should be included per tile, and preferably one for every one or two PV cells. The benefit of this robust design is demonstrated in Appendix A.

7 Conclusions

The purpose of this project was to investigate the feasibility of incorporating photovoltaic cells into roof tiles using injection moulding.

The overall results were as follows. Firstly, the performance of amorphous silicon photovoltaic cells degraded severely during the injection moulding process. The degradation was due to the heat of the process, and progressed with the duration of the process.

Secondly, photovoltaic roof tiles would currently be expensive and would not compete economically with grid-based electricity in South Africa. This was true even if avoided distribution costs, avoided roofing costs and Clean Development Mechanism credits were considered. Other factors such as sustainable development and health benefits could be seen to override the short-term economic losses, though, from a public interest perspective.

The implication of the results was that it would not yet be easy to produce or market injection-moulded plastic photovoltaic roof tiles. This project also revealed some clear positive guidelines for manufacturing photovoltaic roof tiles; especially that more bypass diodes are better, and that glass covers still seem the most appropriate.

Several suggestions for future work are implied. It could be investigated whether the heating time could be reduced to contain the degradation within acceptable limits. This could perhaps be done by faster cooling of the moulded product. Lomold's process is unusual by being quite conducive to a short heating duration.

The effects of perpendicular compression on the amorphous silicon could be investigated. An attempt could at least be made to determine the individual effects of temperature and pressure, not just their combined effects as in this project.

Other photovoltaic technologies could be attempted, such as microcrystalline silicon, cadmium telluride or CIGS. Lastly, the mechanical and chemical appropriateness of plastic for rooftop covers could be investigated more thoroughly.

References

Adelstein, J. *&* Sekulic, B. 2005. Performance and reliability of a 1-kW a amorphous silicon photovoltaic roofing system. In *Proceedings of the 31st IEEE Photovoltaic Specialists Conference and Exhibition*.

Bahaj, A.S. 2003. Photovoltaic roofing: Issues of design and integration into buildings. *Renewable Energy*, 28:2195–2204.

Balenzategui, J.L. *&* Chenlo, F. 2005. Measurement and analysis of angular response of bare and encapsulated silicon solar cells. *Solar Energy Materials & Solar Cells*, 86:53–83.

Berdahl, P., Akbari, H., Levinson, R. *&* Miller, W.A. 2008. Weathering of roofing materials — an overview. *Construction and Building Materials*, 22:423–433.

Builders Trade Depot. 2009. Personal communication on 2 November 2009. Stellenbosch.

Celik, A.N. 2003. Long-term energy output estimation for photovoltaic energy systems using synthetic solar irradiation data. *Energy*, 28:479–493.

Celik, A.N. *&* Acikgoz, N. 2007. Modelling and experimental verification of the operating current of mono-crystalline photovoltaic modules using four- and five-parameter models. *Applied Energy*, 84:1–15.

Czanderna, A.W. *&* Pern, F.J. 1996. Encapsulation of PV modules using ethylene vinyl acetate copolymer as a pottant: A critical review. *Solar Energy Materials and Solar Cells*, 43:101–181.

de Blas, M.A., Torres, J.L., Prieto, E. *&* García, A. 2002. Selecting a suitable model for characterizing photovoltaic devices. *Renewable Energy*, 25:371–380.

Diodes.com. 2009. Online.
Available at: `http://www.diodes.com`

Earth Policy Institute. 1999. Eco-economy indicators. Online. Accessed February 2009.
Available at: `http://www.earth-policy.org`

Erbs, D.G., Klein, S.A. *&* Duffie, J.A. 1982. Estimation of the diffuse radiation fraction for hourly, daily and monthly-average global radiation. *Solar Energy*, 28(4):293–302.

Eskom. 2009*a*. Annual report 2009. Online.
Available at: `http://www.eskom.co.za/annreport09/ar_2009/`

Eskom. 2009*b*. Eskom generation medium term adequacy report. Online.
Available at: `http://www.eskom.co.za`

Eskom. 2009*c*. Tariffs and charges effective from 1 June 2009. Online.
Available at: `http://www.eskom.co.za/tariffs`

Fath, J. 2009. Senior electrical engineer at Eskom. Personal conversation on 22 September 2009.

Filonovich, S.A., Alpium, P., Rebouta, L., Bourée, J.-E. *&* Soro, Y.M. 2008. Hydrogenated amorphous and nanocrystalline silicon solar cells deposited by HWCVD and RF-PECVD on plastic substrates at 150 °C. *Journal of Non-Crystalline Solids*, 354:2376–2380.

Gnucap. 2009. General purpose circuit simulator. Online.
Available at: `http://www.gnu.org/software/gnucap`

Gong, X. *&* Kulkarni, M. 2005. Design optimization of a large scale rooftop photovoltaic system. *Solar Energy*, 78:362–374.

Google Earth. 2009. Online.
Available at: `http://earth.google.com`

Gordijn, A., van den Donker, M.N., Finger, F., Hamers, E.A.G., Jongerden, G.J., Kessels, W.M.M., Bartl, R., van Mol, A.M.B., Rath, J.K., Rech, B., Schaltmann, R., Schropp, R.E.I., Stannowski, B., Stiebig, H., van de Sanden, M.C.M., van Swaaij, R.A.C.M.M. *&* Zeman, M. 2006. Flexible a-Si/μc-si tandem modules in the Helianthos project. In *Conference Record of the 2006 IEEE 4th World Conference on Photovoltaic Energy Conversion*, 4059988, pages 1716–1719.

Gottschalg, R., Betts, T.R., Williams, S.R., Sauter, D., Infield, D.G. *&* Kearney, M.J. 2004. A critical appraisal of the factors affecting energy production from amorphous silicon photovoltaic arrays in a maritime climate. *Solar Energy*, 77:909–916.

Grama, S. 2007. A survey of thin-film solar photovoltaic industry & technologies. Master's thesis, Massachusetts Institute of Technology.

Gueymard, C.A. 2009. Direct and indirect uncertainties in the prediction of tilted irradiance for solar engineering applications. *Solar Energy*, 83:432–444.

Haug, F.-J., Söderström, T., Python, M., Terrazoni-Daudrix, V., Niquille, X. *&* Ballif, C. 2009. Development of micromorph tandem solar cells on flexible low-cost plastic substrates. *Solar Energy Materials & Solar Cells*, 93:884–887.

Hondo, H. *&* Baba, K. 2009. Socio-psychological impacts of the introduction of energy technologies: Change in environmental behaviour of households with photovoltaic systems. *Applied Energy*.

Huld, T., Šúri, M., Dunlop, E., Albuisson, M. *&* Wald, L. 2005. Integration of HelioClim-1 database into PVGIS to estimate solar electricity potential in Africa. In *Proceedings from 20th European Photovoltaic Solar Energy Conference and Exhibition*.
Available at: `http://re.jrc.ec.europa.eu/pvgis/cmaps/afr.htm`

IDES. 2009. Polyamide (nylon) plastic resin. Online.
Available at: `http://www.ides.com/generics/Nylon.htm`

Ishikawa, Y. *&* Schubert, M.B. 2006. Flexible protocrystalline silicon solar cells with amorphous buffer layer. *Japanese Journal of Applied Physics*, 45(9A):6812–6822.

Jaeger, R.C. *&* Blalock, T.N. 2003. *Microelectronic Circuit Design*. 2nd edition. McGraw-Hill.

Jones, R., Johnson, T., Jordan, W., Wagner, S., Yang, J. *&* Guha, S. 2002. Effects of mechanical strain on the performance of amorphous silicon triple-junction solar cells. In *Proceedings of the 29th IEEE Photovoltaic Specialists Conference*, pages 1214–1217.

Kaushika, N.D. *&* Rai, A.K. 2007. An investigation of mismatch losses in solar photovoltaic cell networks. *Energy*, 32:755–759.

Koch, C., Ito, M. *&* Schubert, M. 2001. Low-temperature deposition of amorphous silicon solar cells. *Solar Energy Materials & Solar Cells*, 68:227–236.

Lomold. 2009. Email: info@lomold.com.
Available at: `http://www.lomold.com`

Louw, W. 2009. Personal communication on 18 August 2009. Lomold.

Maroga, J. 2009. Eskom's multi-year price determination — media briefing. Online.
Available at: `http://www.eskom.co.za/live/content.php?Item_ID=11110`

Matsuoka, T., Yagi, H., Waki, Y., Honma, K., Sakai, S., Ohnishi, M., Kawata, H., Nakano, S. *&* Kuwano, Y. 1990. A new solar cell roofing tile. *Solar Cells*, 29:361–368.

Maui. 2009. PV-DesignPro. Maui Solar Energy Software Corporation, Online. Available at: `http://www.mauisolarsoftware.com`

Maycock, P. *&* Bradford, T. 2006. PV technology, performance and cost. Prometheus Institute.

Miles, R.W., Hynes, K.M. *&* Forbes, I. 2005. Photovoltaic solar cells: An overview of state-of-the-art cell development and environmental issues. *Progress in Crystal Growth and Characterization of Materials*, 51:1–42.

Perez, R., Stewart, R., Seals, R. *&* Guertin, T. 1988. *The development and verification of the Perez diffuse radiation model, SANDIA Report SAND88-7030.* Albuquerque, New Mexico: Sandia National Laboratories.

Posnansky, M., Szacsvay, T., Eckmanns, A. *&* Jürgens, J. 1998. New electricity construction materials for roofs and Façades. *Renewable Energy*, 15:541–544.

PowerFilm Solar. 2009. PowerFilm Solar OEM components. Online.
Available at: `http://www.powerfilmsolar.com/products/custom/`

Radziemska, E. 2003. Thermal performance of Si and GaAs based solar cells and modules: a review. *Progress in Energy and Combustion Science*, 29:407–424.

Rath, J.K., Liu, Y., Borreman, A., Hamers, E.A.G., Schaltmann, R., Jongerden, G.J. *&* Schropp, R.E.I. 2008. Thin film silicon modules on plastic superstrates. *Journal of Non-Crystalline Solids*, 354:2381–2385.

Rautenbach, K.F. 2008. Characterisation of a solar roof tile. Master's thesis, Stellenbosch University.

Shah, A.V., Schade, H., Vanecek, M., Meier, J., Vallat-Sauvain, E., Wyrsch, N., Kroll, U., Droz, C. *&* Bailat, J. 2004. Thin-film silicon solar cell technology. *Progress in Photovoltaics: Research and Applications*, 12:113–142.

Silvestre, S., Boronat, A. *&* Chouder, A. 2009. Study of bypass diodes configuration on PV modules. *Applied Energy*, 86:1632–1640.

Skoplaki, E. *&* Palyvos, J.A. 2009. On the temperature dependence of photovoltaic module electrical performance: A review of efficiency/power correlations. *Solar Energy*, 83:614–624.

Smit, R. 2009. Electrical engineer at Eskom. Personal communication on 20 November 2009.

Söderström, T., Haug, F.-J., Niquille, X. *&* Ballif, C. 2009. TCOs for nip thin film silicon solar cells. *Progress in Photovoltaics: Research and Applications*, 17:165–176.

SouthAfrica.info. 2009. Energy. Online.
Available at: `http://www.southafrica.info/business/economy/sectors/energy.htm`

South African Government. 2004. R12,4 million approved for Oudtshoorn housing project. Online.
Available at: `http://www.search.gov.za/`

Spalding-Fecher, R. 2005. Health benefits of electrification in developing countries: A quantitative assessment in South Africa. *Energy for Sustainable Development*, 9(1):53–62.

Stutenbaeumer, U. *&* Mesfin, B. 1999. Equivalent model of monocrystalline, polycrystalline and amorphous silicon solar cells. *Renewable Energy*, 18:501–512.

Sunflare. 2009. Personal communication on 2 November 2009. Sunflare renewable systems.
Available at: `http://www.sunflare.co.za`

Swanepoel, R. 2007. *Renewable Energy Systems 714/814 Course Reader*. Stellenbosch: Centre for Renewable and Sustainable Energy Studies.

Tanda, M., Tabuchi, K., Uno, M., Kato, S., Takeda, Y., Iwasaki, S., Yokoyama, Y., Wada, T., Shimosawa, M., Sakakibara, Y., Takano, A., Nishihara, H., Enomoto, H. *&* Kamoshita, T. 2005. Large-area, light-weight, flexible solar cell production technology — ready for market entry. In *Conference Record of the IEEE Photovoltaic Specialists Conference*, pages 1560–1563.

Ubisse, A. *&* Sebitosi, A. 2009. A new topology to mitigate the effect of shading for small photovoltaic installations in rural sub-Saharan Africa. *Energy Conversion and Management*, 50:1797–1801.

United Nations. 2000. Millenium Development Goals. Online.
Available at: `http://www.un.org/millenniumgoals/environ.shtml`

U.S. Department of Energy. 1999. U.S. Department of Energy Photovoltaics Program. *Energy Efficiency and Renewable Energy Network*. Online. Available at: `http://www.eren.doe.gov`

U.S. Department of Energy. 2000. Carbon dioxide emissions from the generation of electric power in the united states. Online. Available at: `http://www.eiadoe.gov/cneaf/electricity/page/co2_report/co2report.html`

van Dyk, E.E., Audouard, A., Meyer, E.L. *&* Woolard, C.D. 2007. Investigation of the degradation of a thin-film hydrogenated amorphous silicon photovoltaic module. *Solar Energy Materials & Solar Cells*, 91:167–173.

Verkerk, A.D., de Jong, M.M., Rath, J.K., Brinza, M., Schropp, R.E.I., Goedheer, W.J., Krzhizhanovskaya, V.V., Gorbachev, Y.E., Orlov, K.E., Khilkevitch, E.M. *&* Smirnov, A.S. 2009. Compensation of decreased ion energy by increased hydrogen dilution in plasma deposition of thin film silicon solar cells at low substrate temperatures. *Materials Science and Engineering B*, 159–160:53–56.

Woyte, A., Nijs, J. *&* Belmans, R. 2003. Partial shadowing of photovoltaic arrays with different system configurations: Literature review and field test results. *Solar Energy*, 74:217–233.

X-Rates.com. 2009. South African Rands to 1 EUR monthly average 2009. Online. Available at: `http://www.x-rates.com/d/ZAR/EUR/hist2009.html`

Yoshida, T., Tabuchi, K., Takano, A., Tanda, M., Sasaki, T., Sato, H., Fujikake, S., Ichikawa, Y. *&* Harashima, K. 2000. Fabrication technology of a-Si/a-SiGe/a-SiGe triple-junction plastic film substrate solar cells. In *Proceedings of the 28th Photovoltaic Specialists Conference*, pages 762–765.

Zweibel, K. 1999. Issues in thin film PV manufacturing cost reduction. *Solar Energy Materials & Solar Cells*, 59:1–18.

Appendix A: Bypass diode configurations

It seems reasonable that more bypass diodes make a PV installation more modular, and thus more robust, but a quantitative statement is preferable to a 'reasonable' one. Simulations were thus used to show the extent of the benefit of numerous bypass diodes.

An undergraduate investigation by Ubisse & Sebitosi (2009) concluded that, in a module of 36 PV cells, optimum performance was obtained with 6 bypass diodes. This was attributed to the voltage drop over the bypass diodes, which apparently dissipated too much power when there were too many diodes. However the voltage drop over a bypass diode is less than that over a shaded cell that becomes reverse-biased, so their argument needed to be tested. The simulation experiment is detailed in the following section.

A.1 Experimental details

A.1.1 Aim

The aim of this experiment was to simulate a PV module to determine the average effects of different numbers of bypass diodes. The particular aim was to determine if more diodes (up to the number of PV cells) caused better operation or if the module operated optimally with an intermediate number of diodes.

A.1.2 Hypothesis

The null hypothesis was that an intermediate number of bypass diodes, between zero and the number of PV cells, would be optimum. That is, as the number of bypass diodes was increased, the expected power output would increase and then decrease.

Table A.1: Bypass diode configurations in the simulated module

Number of bypass diodes	Length of each string
2	18
4	9
9	4
18	2
36	1

A.1.3 Approach

A PV module of 36 cells was simulated with a number of bypass diodes m_{diodes}. A number of shaded cells m_{shaded} was chosen. Exactly which cells were shaded was made random, and then the expected value of power output and its variability were determined. A higher expected power was considered preferred and so was a lower variability (for consistent operation).

The procedure was repeated for various values of m_{shaded}. When a given module had been characterised well, a new m_{diodes} was chosen, implying a new configuration of bypass diodes.

This approach assumed random shading, but in practice some combinations of shaded cells are more realistic than others, as noted by Ubisse & Sebitosi (2009). However, it is hard to weight the importance of combinations for the general case. Thus random shading with uniform weight was used in this project.

A.1.4 Simulation design

A module with 36 series cells was simulated using Gnucap (2009) as follows. For bypass diodes, a generic model of a 1N4001 power diode was used (Diodes.com, 2009). The characteristics of PV cells from Stutenbaeumer & Mesfin (1999) were used: $I_{\text{L}} = 0.8\,\text{A}$, $I_{\text{o}} = 2{\times}10^{-5}\,\text{A}$, $R_{\text{S}} = 0.2\,\Omega$, $R_{\text{P}} = 100\,\Omega$ and $n = 2.6$. These component choices were largely arbitrary, and did not affect the generality of the results. A single-diode PV cell model was used since this was a power-generating application. Diode breakdown was not simulated since such large voltages were never reached.

A voltage was applied over the module and the resulting current was measured. By applying a range of voltages the module's I-V curve was obtained.

The bypass diodes were applied over strings of cells as listed in Table A.1. One example is shown in Figure A.1 with four bypass diodes.

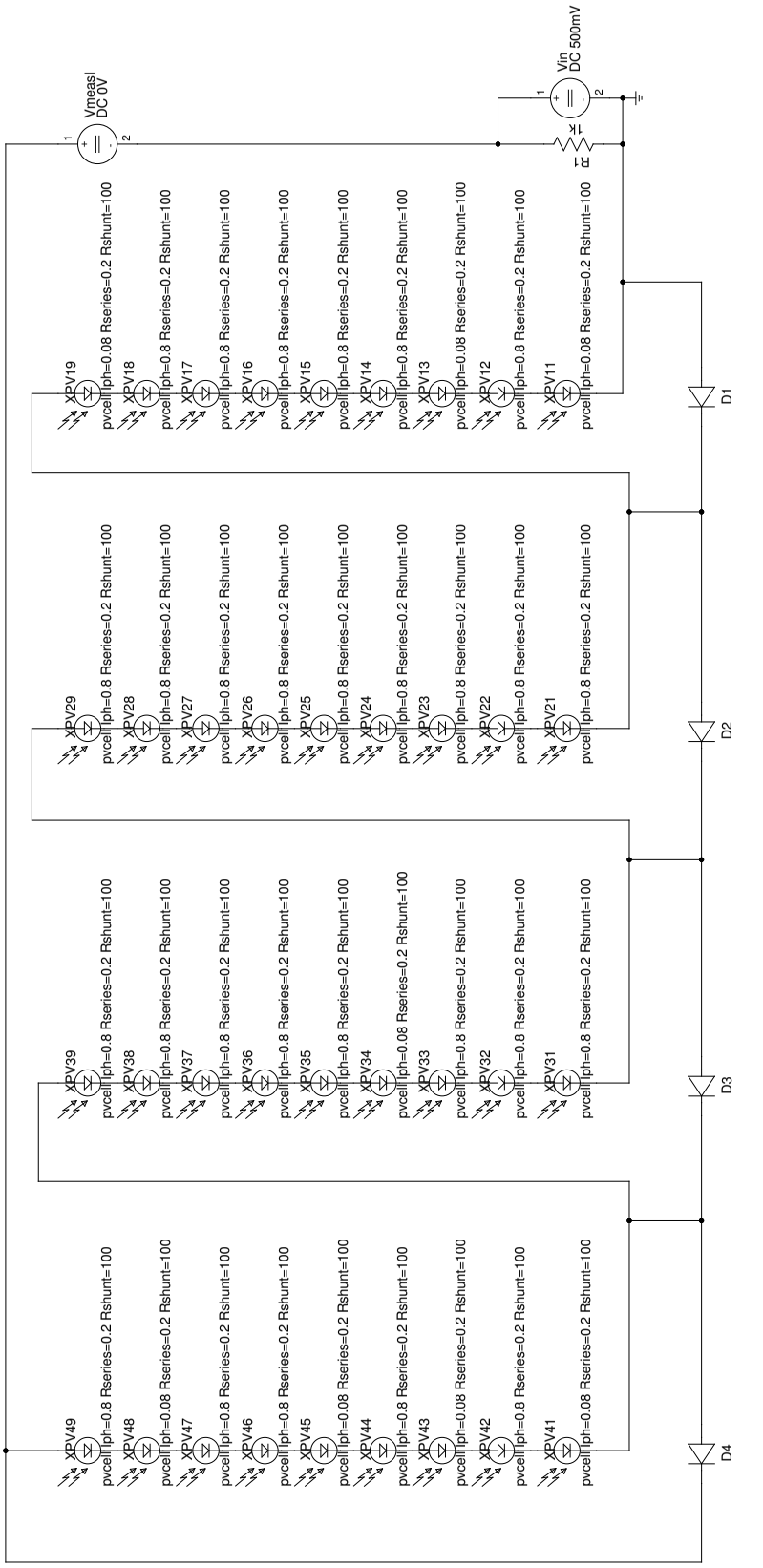

Figure A.1: One example of a simulated module configuration

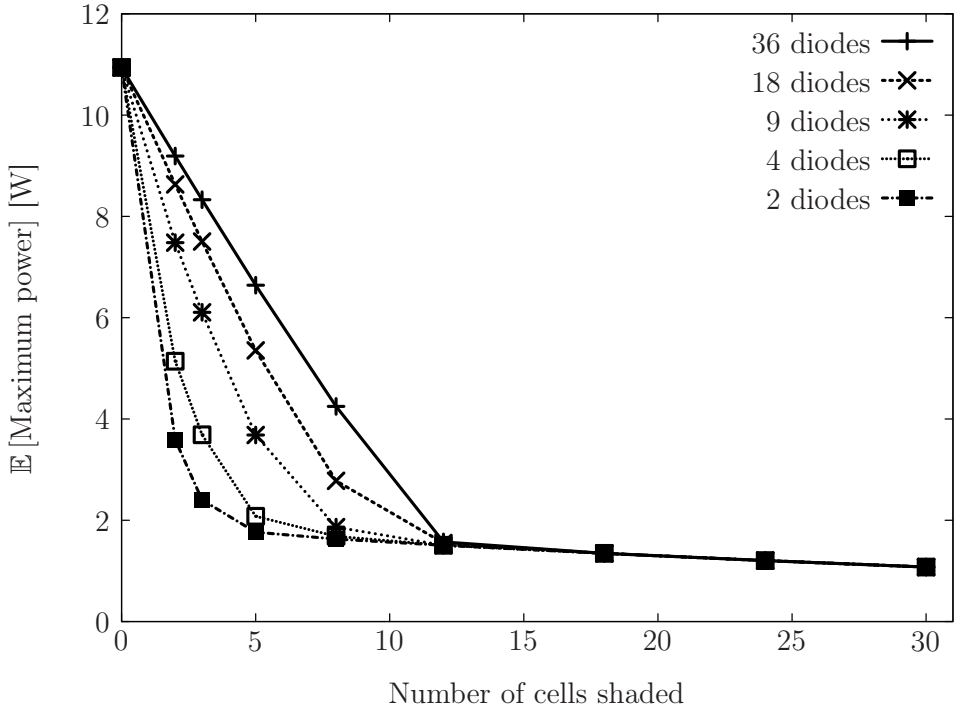

Figure A.2: Simulated effects of shading for various numbers of bypass diodes

Shading was simulated by reducing the current output of random cells to a tenth of their normal value. In the case of Figure A.1 there were 8 shaded cells, identified by '`Iph=0.08`'. In a similar way each time, m_{shaded} were shaded. A hundred such random scenarios were simulated for each m_{shaded}, and the maximum power extracted every time. The mean of these powers gave the expected value of power output. The standard deviation gave some measure of the variability of power output.

A.2 Results

The expected power output is depicted in Figure A.2. The main result is clearly evident, that the expected power output was always higher when more bypass diodes were used. The null hypothesis, of an intermediate number of diodes being optimal, was clearly wrong. It can also be seen that as more cells were shaded the expected power decreased towards an asymptotic value. This value was a tenth of the module's unshaded power output, consistent with partial shading as simulated.

An interesting result was that no benefit from bypass diodes was achieved when 12 or more cells were shaded. This was due to more than one cause. In the case of 36 bypass diodes the voltage drop over them nulled the voltage generated

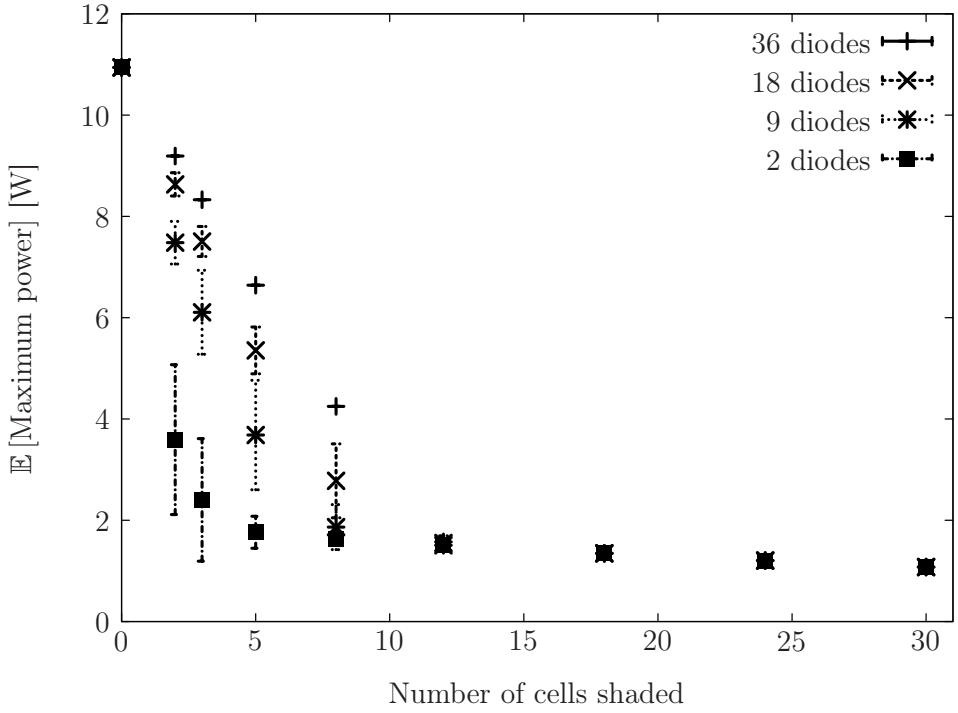

Figure A.3: Variability of the effects of shading for various numbers of bypass diodes

by the active cells. (The diode drop of the 1N4001 was 0.9 V at a current of 0.8 A, greater than the voltage of the cells $V_{\mathrm{m}} \approx 0.51\,\mathrm{V}$; although both varied with the changing maximum power point.) In the case of 2 bypass diodes the probability of only one series string being affected was so low when 12 cells were shaded that it hardly affected the expected power. (The probability was $3{\times}10^{-5}$, calculated using the hypergeometric distribution.)

The variability of the power output is shown in Figure A.3, where one bypass diode configuration has been omitted for clarity. The vertical lines show the maximum power's standard deviation for each random shading case; they do not represent the maximum or minimum value encountered. The main result was that there was more variability when less bypass diodes were used. This is understandable as in the case of 2 bypass diodes, where the only possibilities are that half the module is working or none of it is.

The vertical lines in the figure fall short of the higher values of expected output. This shows that for most cases, even though they have greater variability, the configurations with fewer bypass diodes would not do as well in practice. It should be remembered, though, that random shading was simulated here, and in special cases different diode configurations may still make sense.

A.3 Conclusion

More bypass diodes, up to the number of cells in the module, improve the operation of a PV module. More diodes give a higher expected output power and a lower variability under random shading. However, there is no real benefit due to bypass diodes when more than a critical number of cells is shaded.

Appendix B: PV-DesignPro simulation of a PV system

The PV-DesignPro computer program (Maui, 2009) was used to simulate the energy output of the PV system for a single house in the fictional housing project of Section 5.

B.1 Simulation inputs

PV-DesignPro is designed to simulate photovoltaic systems to determine their effectiveness throughout the year. The basic algorithm it uses is the 'typical meteorological year'. A database of irradiance, temperature and wind speed for one whole typical year is used. The irradiance is calculated from the clearness index. To determine the irradiance on the tilted modules, the anisotropic diffuse irradiance model of Perez *et al.* (1988) is used.

For this simulation a data set for Cape Town's weather was used. The other inputs were divided into different categories which are described and justified below.

Array A suitable a-Si module was chosen from the available options. It was the Solarex MST-43LV 1998 model, which was appropriate because it was also double-junction, and its voltage and efficiency were similar to the PowerFilm modules. Its power output was much larger than one of the PowerFilm modules, though, so only 24 Solarex modules were used as an approximation to 656 PowerFilm modules.

The mismatch losses for series and parallel connections were lumped together as a 0.84 % derating factor for the array current [calculated using Equation (5.1)].

The tilt was chosen as 32°, which is the optimum for the Cape Town region according to Huld *et al.* (2005). That meant the roof trusses would have to be specially chosen to tilt at 32°, and might have to be specially manufactured. A mono-pitched roof truss as in Figure B.1

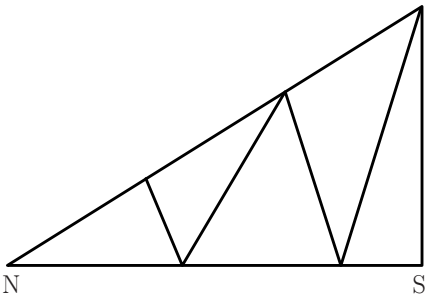

Figure B.1: A mono-pitched roof truss facing north

would make the best use of the roof space because any south-facing slope is not appropriate for PV tiles.

Load The load was assigned arbitrarily, but with peaks in the morning and evening times. The main constraint was that the load added up to 4 kWh per day; the designed output of the PV system.

When the batteries discharged below 45 % then the load was disconnected in the simulation. The batteries were allowed to charge back to 75 % before the load was again given power. That is, no backup power source was simulated.

Shading Shading was assumed to be negligible due to the houses being spaced far enough apart and not being surrounded by large trees. This was reasonable since the sun always rises fairly high above the horizon in the Western Cape region. It rises above 20° in a matter of less than 2 hours, even in winter, and would produce a comparatively small amount of energy during this time at these low angles.

Batteries The battery chosen was the IBE BY/IB3-55N-11. It was rated to store 412 Ah at 6 V, so 8 batteries were placed in series to provide 48 V for the inverter.

Inverter No inverter was found in the database similar to that designed and priced in Section 5. A new entry was thus made with the typical specifications of the quoted Outback FX 3048T. The inverter consumed 23 W during operation and 6 W when idle. Its efficiency was 93 % (assumed the same at all loads).

B.2 Results

The PV system performed well throughout the year, with some periods of no supply ('down-time') during winter.

Month	Load Wh	Backup Wh	Charging Wh	PV+Wind Wh	Solar Fraction	Max SOC	Ave SOC	Min SOC
JAN	147 810.33	0.00	0.00	147 810.33	100.00%	99.97	86.84	72.02
FEB	133 506.11	0.00	0.00	133 506.11	100.00%	96.03	85.79	66.78
MAR	147 810.33	0.00	0.00	147 810.33	100.00%	95.37	83.43	60.46
APR	143 042.26	0.00	0.00	143 042.26	100.00%	93.68	70.35	52.87
MAY	147 810.33	27 532.06	0.00	120 278.27	81.37%	86.01	63.26	44.99
JUN	143 042.26	34 718.17	0.00	108 324.08	75.73%	86.81	60.94	44.99
JUL	147 810.33	32 044.79	0.00	115 765.54	78.32%	84.34	63.84	44.99
AUG	147 810.33	22 963.73	0.00	124 846.60	84.46%	88.59	66.08	44.99
SEP	143 042.26	5 302.89	0.00	137 739.37	96.29%	94.19	75.64	44.99
OCT	147 810.33	0.00	0.00	147 810.33	100.00%	95.58	78.86	53.94
NOV	143 042.26	0.00	0.00	143 042.26	100.00%	96.96	85.68	66.11
DEC	147 810.33	0.00	0.00	147 810.33	100.00%	96.17	85.38	63.16
YEAR	1 740 347.47	122 561.65	0.00	1 617 785.83	92.96%	99.97	75.51	44.99

Figure B.2: PV-DesignPro simulation output: Performance table

The performance table is shown in Figure B.2, where it can be seen that the energy output for the year was 1618 kWh. This output, however, was that of the idealised system before taking into account efficiency losses of the inverter, batteries and cabling. During January, when there was no down-time, the load received 124 Wh and the supply was shown to be 148 Wh, indicating efficiency losses of 16.1 %. This suggested the system's actual output for the year was 1357 kWh.

The system provided 93 % of the load's requirements over the course of the year, as shown in Figure B.3. The down-times during winter were caused by less sunlight than the designed amount when there were, for example, consecutive cloudy days. This could be compensated for by oversizing the PV array. This is not recommended because the cost per unit energy would be increased, as the excess capacity would not be used during summer. As Celik (2003) notes, preventing down-time completely requires heavily oversizing the system.

An example of one period when the battery discharged to below 45 % is shown in Figure B.4 on page 73. The battery discharged during consecutive cloudy days shown by low irradiation in the top graph. It was recharged during sunny days before the load was resupplied with power. This kind of cut-off may only be a nuisance in a residential context, but probably needs to be dealt with in a commercial context.

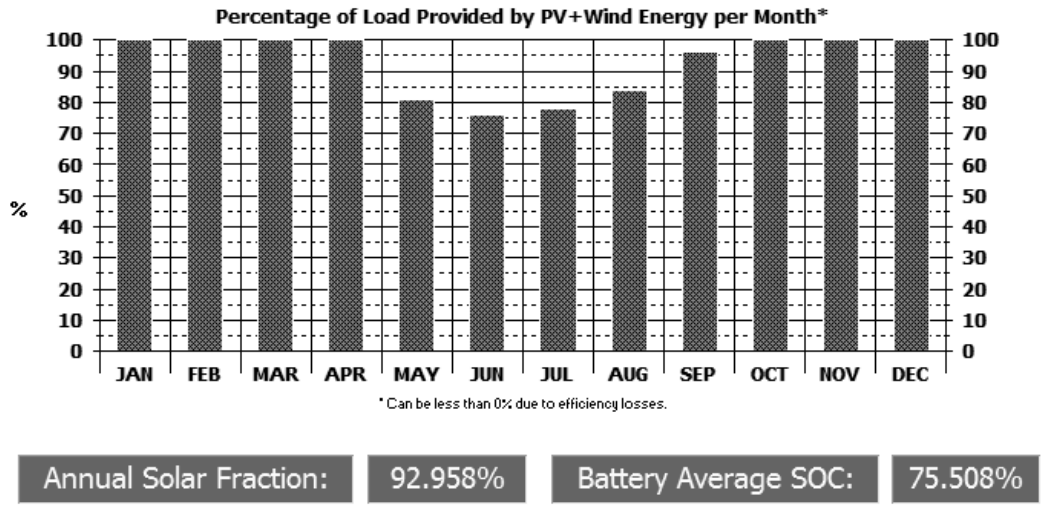

Figure B.3: PV-DesignPro simulation output: Solar fraction

B.3 Possible variations

Some of the inputs to the simulation were determined on a trial-and-error basis. The following variations gave some insights.

Standardised roof tilt The precise tilt angle is not very important. If a standardised roof tilt angle of 30° was used, instead of 32°, then the energy produced in the year was reduced by 0.4 %. For a tilt angle of 25° the energy was reduced by 1.7 %.

South-facing slope Placing PV tiles on a south-facing slope is very ineffective. The array was simulated facing south for comparison and the energy output was reduced by 42 %.

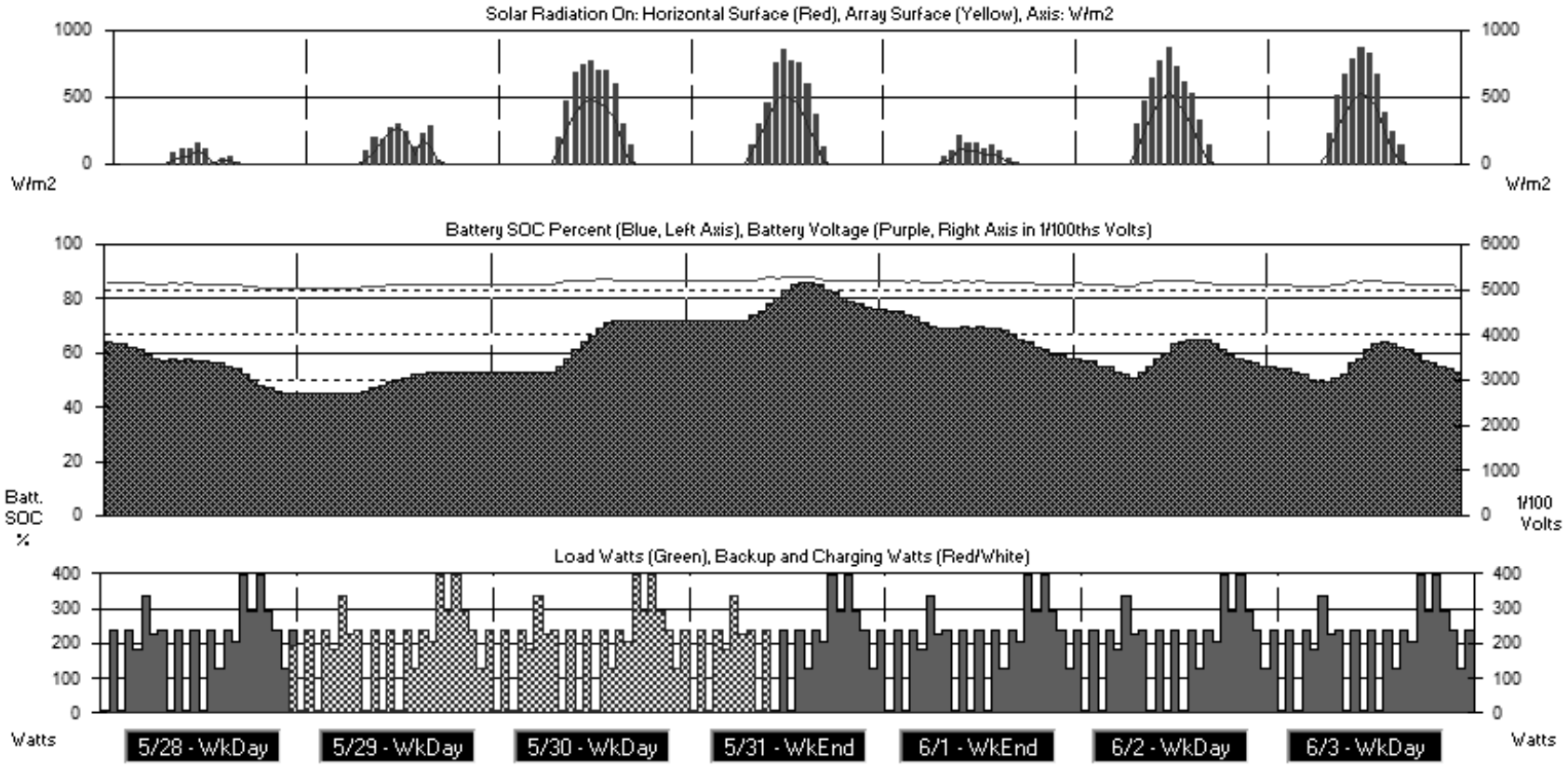

Figure B.4: PV-DesignPro simulation output: Battery charge status during a week in winter